KRISO
KOREA RESEARCH INSTITUTE OF SHIPS & OCEAN ENGINEERING

Pacific Community
Communauté du Pacifique

Preliminary Feasibility Study of Ocean Thermal Energy Conversion Application in Kiribati Waters

April 2016

Geoscience Division of the Pacific Community
SPC00038

Zulfikar Begg and Robert Smith[1]

Disclaimer

While care has been taken in the collection, analysis, and compilation of the data, it is supplied on the condition that the Geoscience Division of the Pacific Community shall not be liable for any loss or injury whatsoever arising from the use of the data.

[1]Geoscience Division of the Pacific Community

Preliminary Feasibility Study of Ocean Thermal Energy Conversion Application in Kiribati Waters

Zulfikar Begg and Robert Smith

Pacific Community
Communauté du Pacifique

Suva, Fiji 2016

SPC00038

Original text: English

Prepared for publication at SPC's Suva Regional Office, Private Mail Bag, Suva, Fiji, 2016
www.spc.int

TABLE OF CONTENTS

LIST OF TABLES AND FIGURES

ACKNOWLEDGMENTS

This report was successful due to the contribution of a large number of people who assisted during field surveys and data processing.

Much appreciation and gratitude goes to the following organisations and individuals:

- Ministry of Public Works and Utilities, Kiribati
- Ministry of Environment, Lands and Agricultural Development, Kiribati
- Dr Cyprien Bosserelle, Geoscience Division, Pacific Community
- Herve Damlamian, Geoscience Division, Pacific Community
- Christopher Mark Day, Geoscience Division, Pacific Community

Pacific Community Survey Team:

- Robert Smith, Senior Advisor Marine Geophysics
- Zulfikar Begg, Senior Technical Assistant
- Poate Degei, Technical Officer
- Donato Roqica, Technical Officer

Korea Research Institute of Ships and Ocean Engineering Survey Team:

- Hosaeng Lee, Senior Researcher
- Jahun Jung, Manager GEMATEK Co, Ltd
- Seungtaek Lim, Project Based Researcher
- Yongkeuk Ham, Senior Researcher
- Youngkyo Seo, CEO GEMATEK Co, Ltd
- Jungyoon Yeo, Manager GEMATEK Co, Ltd

ABBREVIATIONS

CTD:	conductivity, temperature, depth
ENSO:	El Niño Southern Oscillation
GDP:	generalised pareto distribution
GEBCO	general bathymetric chart of the oceans
IPCC:	Intergovernmental Panel on Climate Change
ITCZ:	intertropical convergence zone
KRISO:	Korean Research Institute of Ships and Ocean Engineering
OTEC:	ocean thermal energy conversion
POT:	peak over threshold
SEAFRAME:	sea-level fine resolution acoustic measuring equipment
SPC:	Pacific Community
SSS:	sea surface salinity
SST:	sea surface temperature

EXECUTIVE SUMMARY

Most Pacific island countries have begun committing to other sources of energy other than fossil fuels with the mind-set to curb emissions and to utilize local resources. In search of sustainable energy, developing island nations have begun using renewable sources of energy.

The Preliminary Feasibility Study for Ocean Thermal Energy Conversion Application project, funded by the Korean Research Institute of Ships and Ocean Engineering, involved the Geoscience Division of the Pacific Community to complete phase 1 and 2 activities of the project.

Previous studies on thermocline, ocean conditions, and wind and wave conditions were reviewed and documented. Relevant data from previous surveys such as conductivity, temperature, depth, bathymetry and tide gauge data were reviewed and collated.

Argo profile data was downloaded and analysed. Argos data for Tarawa (Kiribati) waters was recorded by 51 stations from 2004 to early 2015. Analyses and comparisons were made on the temperature profiles with depth. No significant variation was observed and temperature against depth profile illustrated a similar trend of all profiles.

An activity summary of the final field mission to Tarawa has also been documented.

1 INTRODUCTION

1.1 Background

The Preliminary Feasibility Study for Ocean Thermal Energy Conversion (OTEC) Application project was proposed for Kiribati in partnership with the Geoscience Division of the Pacific Community (SPC) and the Korean Research Institute of Ships and Ocean Engineering (KRISO).

OTEC is an auspicious, viable and renewable source of energy that exploits the ocean's thermal gradient — the difference between warm surface water and cold deep seawater — to generate electricity. The technology involves generating electricity by transforming heat derived from temperature differences between the deep ocean (~ 1000 m depth) and surface waters (up to 20 m depth). A minimum of 20°C in temperature difference is needed for an OTEC system to function efficiently.

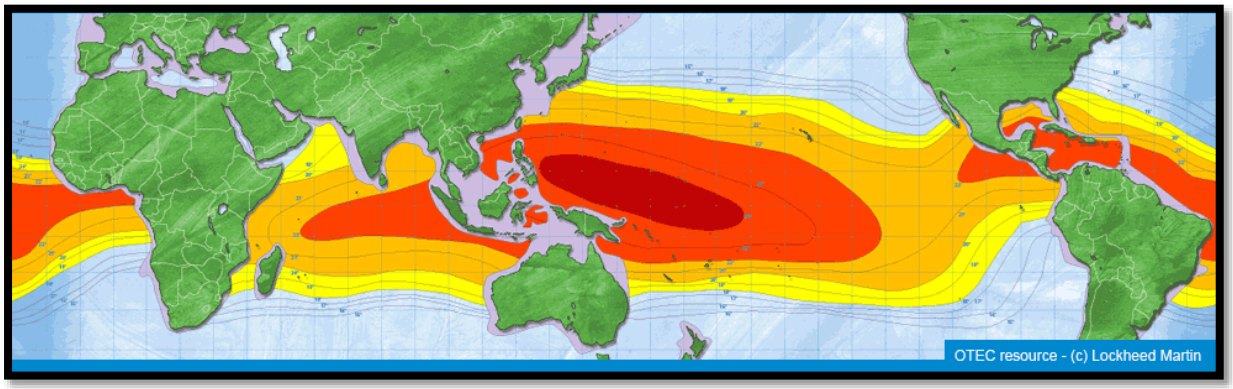

Figure 1: The OTEC technology is viable in the equatorial regions as annual temperature differential is at a minimum of 20°C. Map shows temperature contours (isotherm) of the ocean around the equator, sourced from http://www.otecnews.org/.

The OTEC technology has been in operation in a number of countries. Some recent examples are: Indian Navy's go green initiative using the OTEC plant: **http://www.otecnews.org/2015/12/indian-navy-plans-to-go-green-with-otec-at-andaman-nicobar-islands/** World's largest OTEC plant connected to grid in Honolulu: http://www.otecnews.org/2015/08/worlds-largest-otec-plant-connected-to-grid/

1.2 Project objectives and outcomes

The project aims to evaluate the feasibility of an OTEC facility in Kiribati and, hence, the main objectives are to review and assess relevant data and identify gaps and quality of data required for this pilot project. Analysis will also be completed with regards to socioeconomic and energy demand of Tarawa to highlight the viability of OTEC technology.

This project is a preliminary assessment and includes two phases:

- Phase 1: A desktop study to identify relevant data (with SPC) that could assist the feasibility study and identify gaps with regard to phase 2 activities; and
- Phase 2: A reconnaissance study of the proposed project site.

1.3 Purpose of this report

This report describes oceanographic conditions such as bathymetry, temperature gradients, and extreme wind and wave analyses for Tarawa, particularly for the selected project sites.

1.4 Site description

The Republic of Kiribati (hereafter referred to as simply Kiribati), in the central Pacific, consists of 1 raised coral island and 32 atolls among three island groups (Gilbert, Line and Phoenix), which together cover an ocean area of 4,200 km east to west and 2,000 km north to south with a total land area of 811 km^2.

The population of Kiribati is 103,058 (Kiribati National Statistics Office, 2010) and the overall population growth rate is 2% per year.

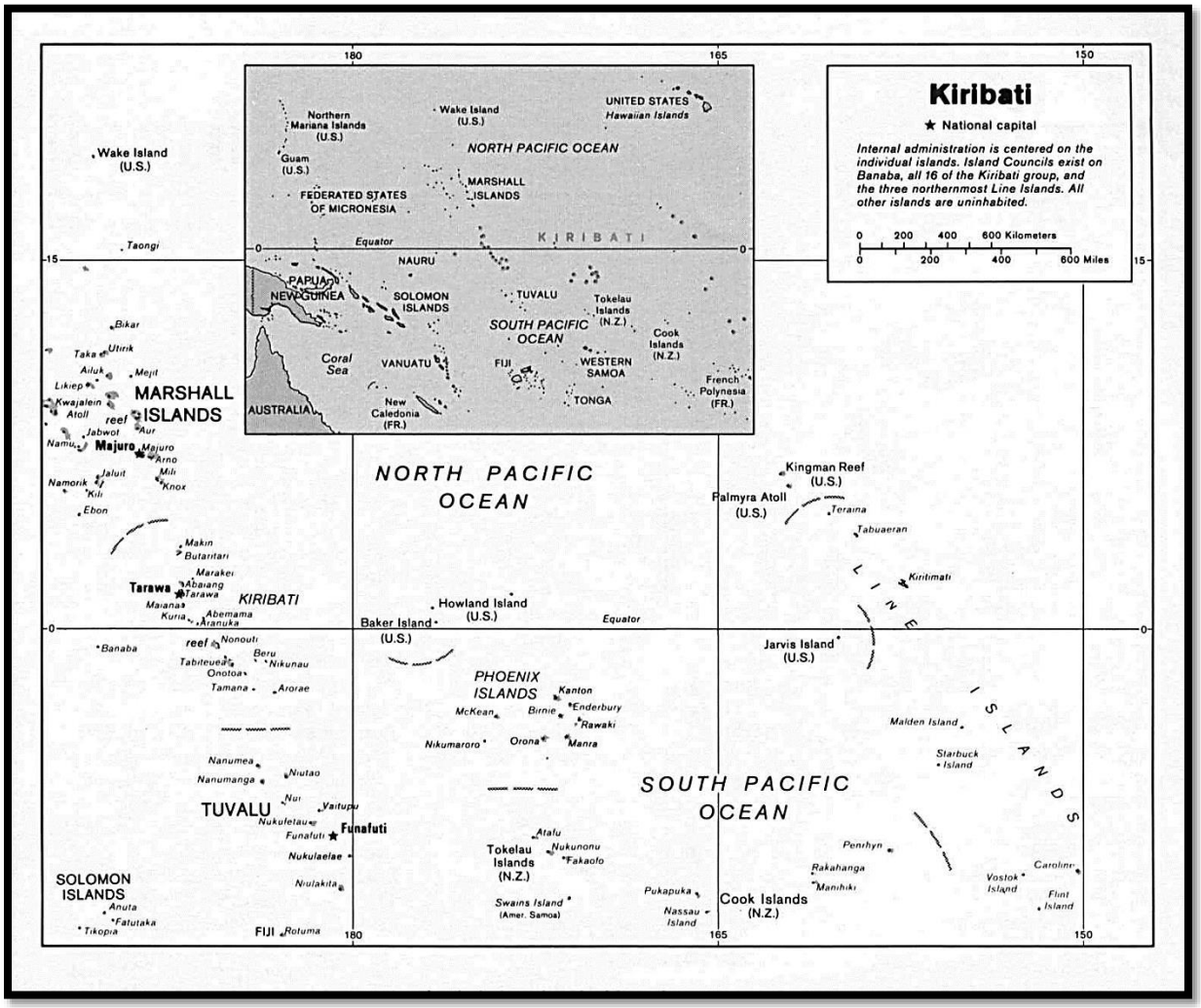

Figure 2: Map of the Pacific showing the location of the Kiribati Group. Source: http://geography.about.com/od/kiribatimaps/

Kiribati's climate is hot and humid, with very little variability in air temperature, which is mostly in equilibrium with ocean surface temperatures surrounding the atolls. Variations in air temperature from season to season are mainly below 1°C.

Figure 3: Tarawa Atoll and the three proposed study sites. Point 1 is west of Betio, Point 2 is south of Betio (causeway connecting to Bairiki), and Point 3 is south of Temaiku. Points are projected on a Google backdrop.

2 MAIN CONTEXT

2.1 Thermocline evolution with El Niño Southern Oscillation in the Pacific region

The Intergovernmental Panel on Climate Change (IPCC) 2013 report defines the thermocline as the layer representing the maximum vertical temperature gradient in the ocean that is bounded by the ocean's surface and the abyssal zone. In subtropical regions, the thermocline is represented in surface waters, whereas in higher latitudes it is at times absent and is replaced by layer of maximum vertical salinity gradient.

The equatorial Pacific ocean-atmosphere system has been noted by many authors (e.g. Galanti et al. 2002; Battisti and Hirst 1989; Hirst 1986; Philander 1983) to be in an instable state, which is one of the major factors driving the extent of the El Niño Southern Oscillation (ENSO) and permitting the evolution of atypical conditions resulting in El Niño and La Niña events (Galanti et al. 2002). ENSO phenomena occur globally, with a strong interaction between the tropical ocean and the earth's atmosphere.

A major factor driving the strength of the instable ocean-atmosphere system is the seasonal movement of the Pacific intertropical convergence zone (ITCZ) (Philander 1983). Added climatological factors enhancing the combined ocean-atmosphere instability are large zonal gradients of mean sea surface temperature (SST), shallow thermocline, strong zonal winds, high SST (Hirst 1986) and strong upwelling (Battisti 1988).

Galanti et al. (2002) report on the variances in the thermocline in the Pacific. During the season from summer to early winter, there is a strong correlation with the surface thermocline and anomalies that arrive as Kelvin waves from the west, and from late winter to early spring when the thermocline outcropping is at its minimal; temperature anomalies do not affect much and dispel within the thermocline.

Holbrook and Bindoff (1998) also highlight the suitability of a temperature-based proxy for understanding thermal variability. They used the 13°C and 14°C isotherm to represent the thermocline in the South Pacific Ocean.

During the month of March, when the near surface temperature waters are cooler, the thermocline is elevated, whereas in October when the surface temperatures are warmer, the thermocline is constrained (Figure 4). Holbrook and Bindoff (1998) established that vertical motions of the thermocline, coupled with seasonal temperature anomalies in the southwest Pacific, were independent of an "annual cycle of solar insolation".

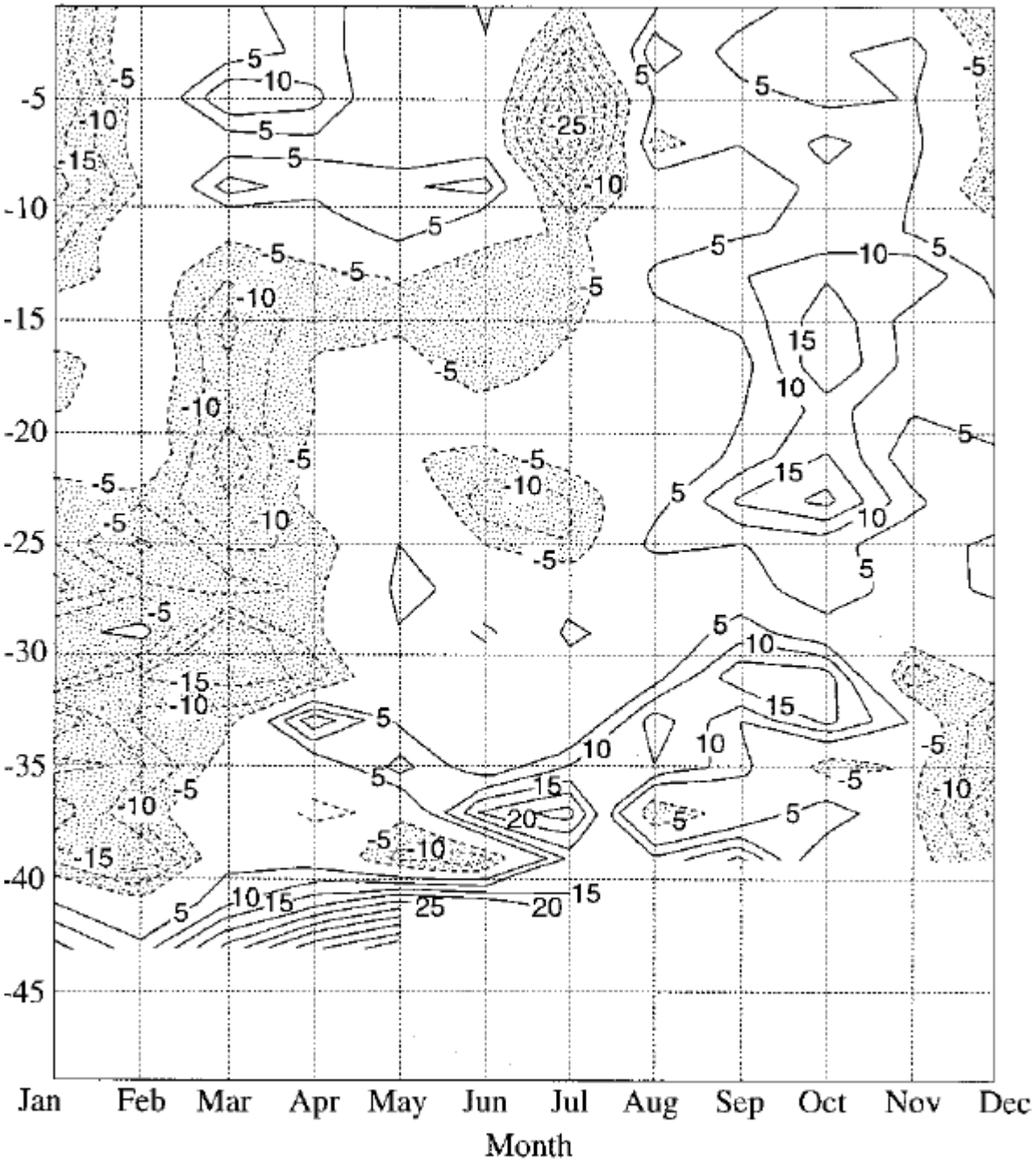

Figure 4: Hovmöller plot adapted from Holbrook and Bindoff (1998), showing the mean anomalies derived from annual mean values based on isotherm depths of 14°C (equatorward of 36°S) and 13°C (poleward of 36°S). Depths are in meters and positive anomalies show that the isotherms are deeper.

The thermocline structure in the Pacific has been described by Sverdrup dynamics, particularly Sverdrup pressure from recorded wind stress, which illustrates that during periods of high atmospheric pressure, the thermocline is deep, and is shallow during periods of low atmospheric pressure (Kessler et al. 2003; Landsteiner et al. 1990; Leech et al. 2013; Munk 1950; Sverdrup 1947).

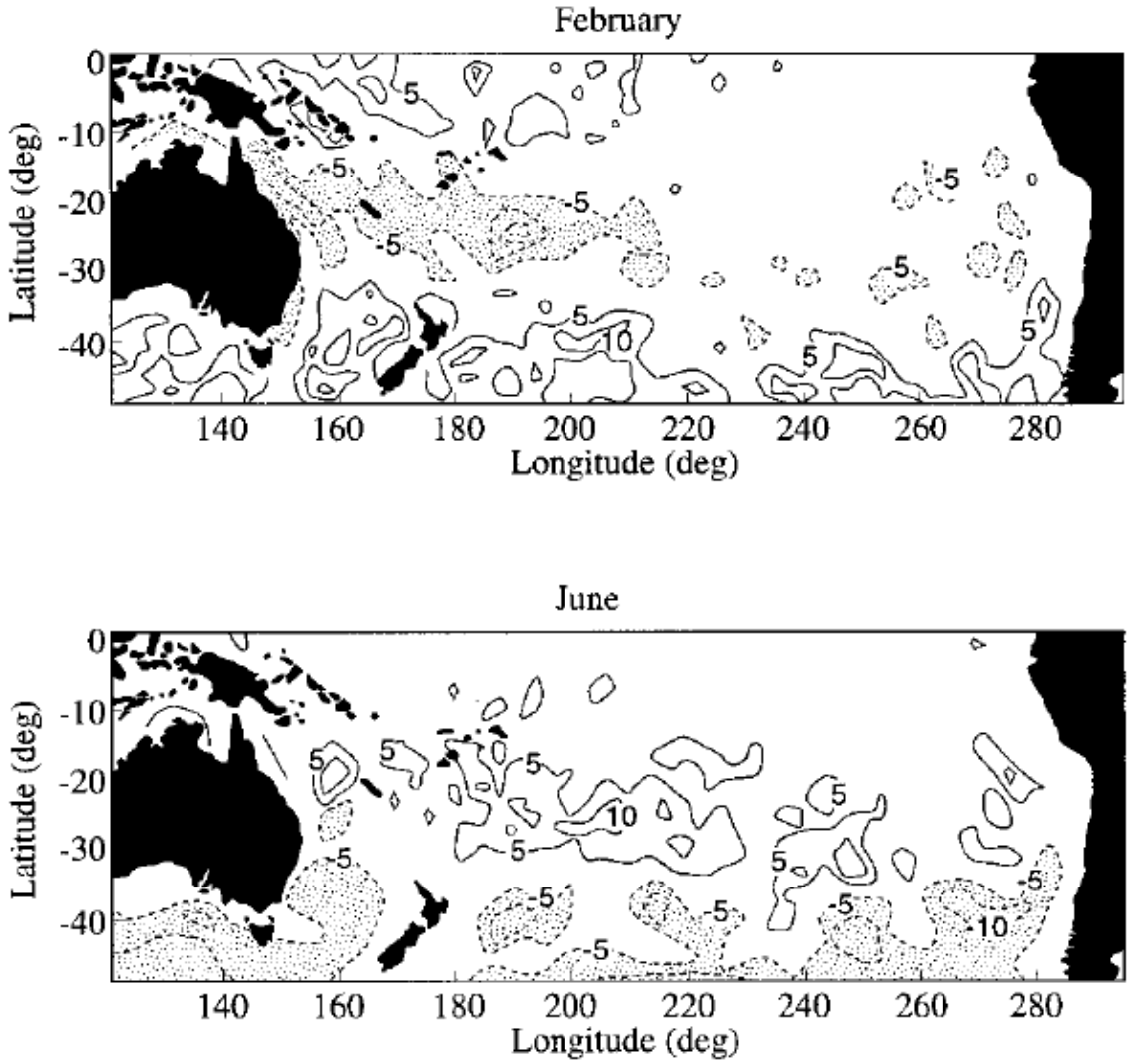

Figure 5: Wind stress curl anomalies across the South Pacific Ocean for the months of February and June (peak periods of anomalies). The stress anomalies are in units of 10^{-8} N m^3 and were calculated by Holbrook and Bindoff (1998).

Sverdrup pressure is controlled by 'zonal wind stress', which results in the tilting of the thermocline farther down to the west, and 'wind stress curl', which causes the thermocline to raise upwards where the wind field is divergent and expands the thermocline where it is convergent. Although wind stress curl influences the thermocline depth, local conditions also contribute towards the development of the thermocline across the Pacific (Leech et al. 2013).

The advancement of wind stress curl anomalies has been discussed by Holbrook and Bindoff (1998) and is illustrated in Figure 5. The anomalies spread in a northwest to southeast orientation into the central Pacific.

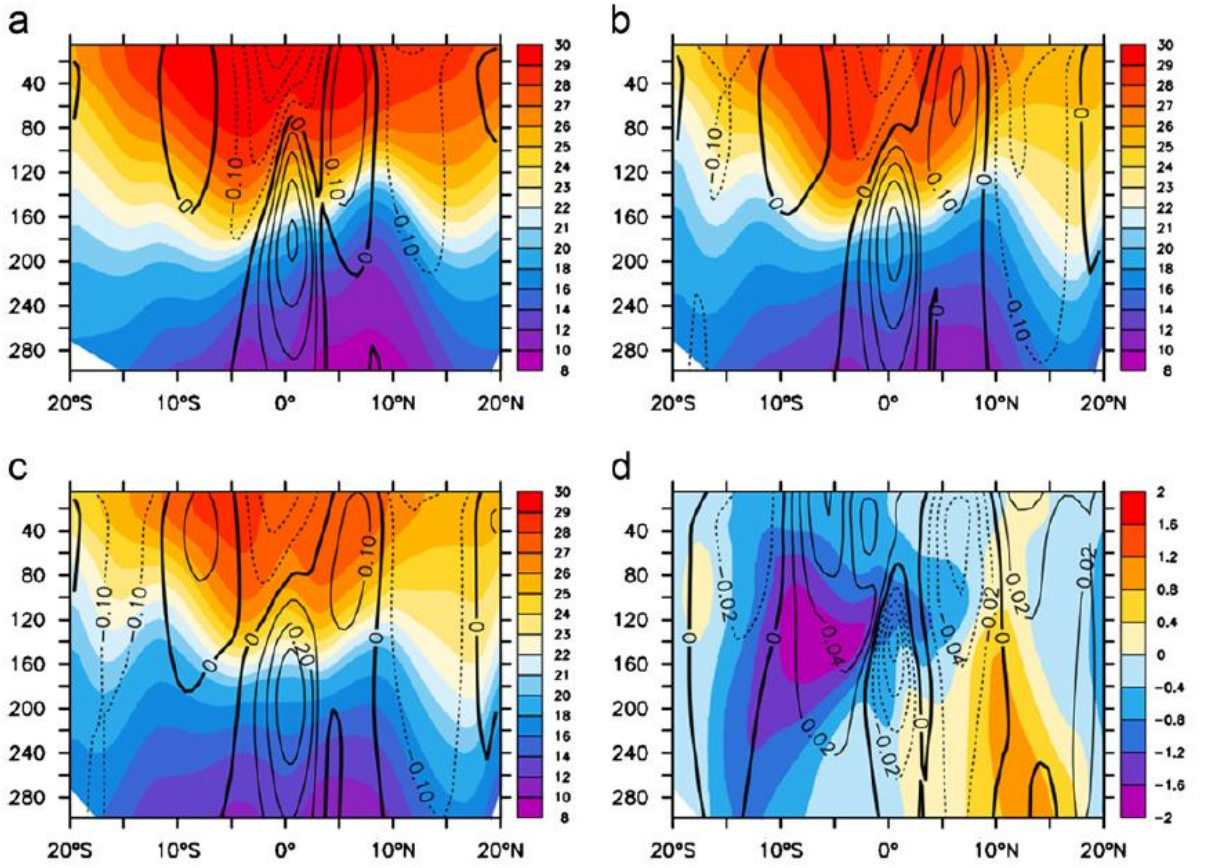

Figure 6: Vertical cross section of ocean showing temperature °C (in colours) from 0–300 m at longitude 160°E. Contours represent zonal flow with an interval of 0.02 m/s. a) observed profile; b) 40-year average from Geophysical Fluid Dynamics Laboratory GFDL's, Community Climate Model Version 2 (CM2.0) model control' c) 40-year average from GFDL's CM2.0 model perturbed experiment with imposed anomalous freshwater flux over the northern North Atlantic. D shows the difference between (c) and (b).Source: Leech et al. (2013) and used with permission.

A Northern Hemisphere thermocline ridge is produced in the western Pacific from the divergent wind stress curl just north of the ITCZ, resulting in the ridge following the movements of the ITCZ (i.e. if the ITCZ moves north or south, the ridge moves north or south). A much weaker ridge than the northern ridge is formed in the central Pacific due to the large area of converging wind stress curl (Figure 6. The pattern of wind stress curl in the Southern Hemisphere creates shoaling and results in a smaller thermocline ridge (Leech et al. 2013).

Figure 7 illustrates the ENSO phenomena and the respective change in the thermocline structure. During La Niña conditions, the SST declines below normal average temperature, causing the thermocline to become deeper. During El Niño conditions there are periods of marked warmer SST, which induces a shallower thermocline anomaly and also produces a more flattened thermocline compared with normal conditions when there is a steep thermocline tilt from East to West.

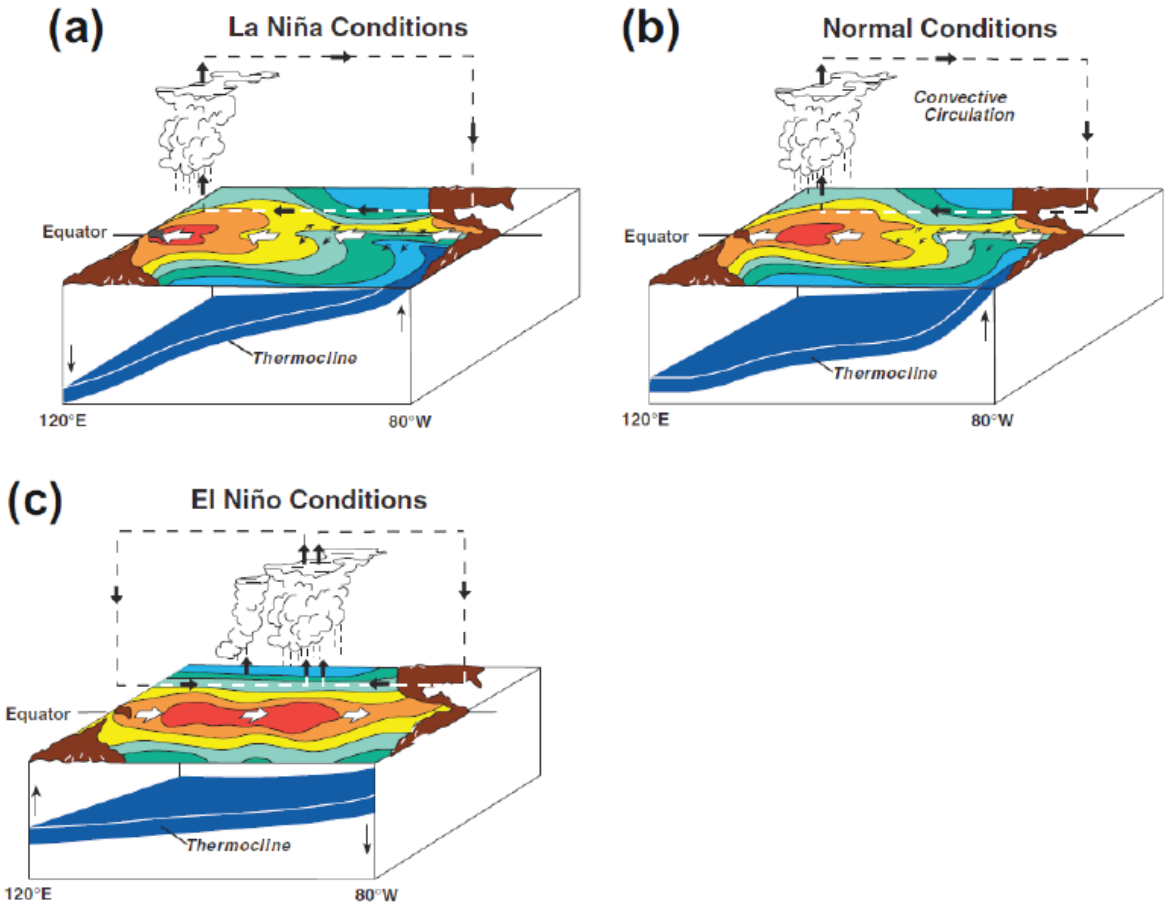

Figure 7: Structure of the thermocline during ENSO: a) the thermocline during La Niña conditions; b) thermocline in normal conditions; and c) thermocline during El Niño conditions. Source: Talley et al. 2011.

2.2 General oceanographic conditions

Majority of the oceanographic and water quality studies conducted in Tarawa has focussed on the lagoon side therefore, very little or oceanographic data is available for the ocean side of Tarawa Atoll where three potential locations for an OTEC plant to be sited with respect to the ocean side of South Tarawa, as illustrated in Figure 3.

Kiribati's climate is governed by the ocean, with Tarawa situated in a region of equatorial upwelling. Ocean surface temperatures range from 27°C to 29°C and sea surface salinities ranging from 35.2 ppt to 36.0 ppt. The major ocean current around Tarawa are the south equatorial currents, which have an easterly set around the atoll. Tidal exchanges between the ocean and the lagoon play a key role in controlling water quality and productivity. The ocean transports nutrients to biota in the lagoon and also flushes lagoon waters.

Naidu et al. (1991) surveyed Tarawa's lagoon as part of a water quality assessment. Dissolved oxygen readings ranged from 9.8 mg/L to 10.8 mg/L, signifying the saturation of oxygen within the lagoon. Ammonia, nitrate and phosphate levels were also measured, and these were not significant compared with their respective detection levels.

2.2.1 Extreme wave and wind analysis

Wave conditions for the surrounding Betio area (ocean side) has been described by Bosserelle and colleagues (2015). The yearly average wave height was noted to be 0.79 m with a mean direction of 208° and an annual mean wave period of 12.18 s, Table 1(Source: Bosserelle et al. 2015

).

Table 1: Mean wave conditions for Betio, Tarawa calculated from 1979 to 2012.

Mean wave height	0.79m
Mean wave period	12.18s
Mean wave direction [° True North]	208 °
Mean number of wave components	7.21
Mean annual variability [m] (%)	0.05 m (6.2 %)
Mean seasonal variability [m] (%)	0.22 m (27.7 %)

Source: Bosserelle et al. 2015

Bosserelle et al. (2015) reported on the inconsistent wave pattern throughout the year for Betio, which is influenced by seasonal changes in wind patterns. Figure 8 shows the monthly variation of wave conditions for Betio, with 27% variability in wave height. Sites exposed to trade winds show smaller variation compared with sites exposed to North Pacific swell, which has a monthly variation greater than 30%.

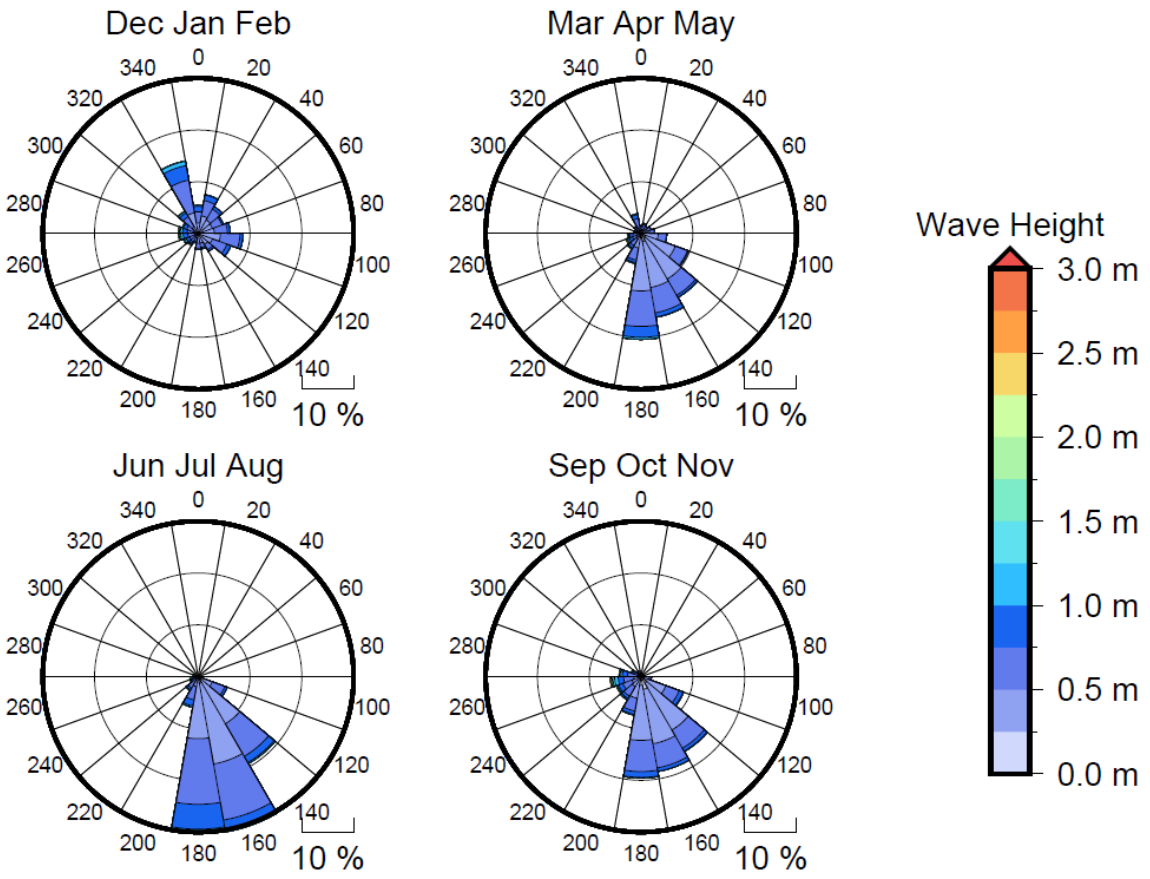

Figure 8: Seasonal wave rose for Betio, Tarawa Atoll. Adapted from Bosserelle et al. 2015.

The main direction for waves around Betio is from the south for all the seasons, except during the winter when the direction is from the north. Seasonal changes impede on wave heights, hence the mean wave height is based on and changes with the season.

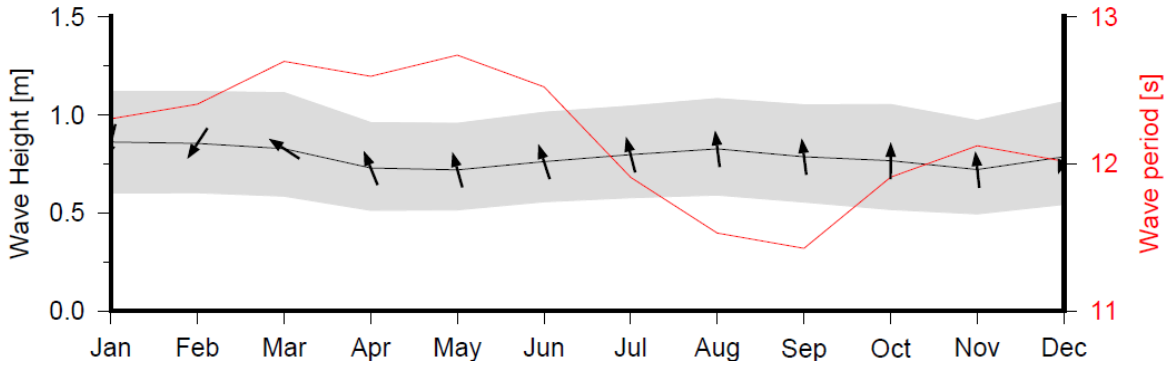

Figure 9: Wave conditions in Betio modelled by Bosserelle et al, (2015) for the respective months. The black line indicates wave height, red line illustrates wave period, and arrows indicate wave direction.

Bosserelle et al. (2015) mention the interannual variability for wave height (6.2%) for Betio, which has remained unchanged since 1979. The authors also higlighted that the mean annual wave height is associated with ENSO, and is quite evident in wave conditions around the Pacific (e.g. changes in wave condtions during the 1997/1998 El Niño as shown in Figure 10.

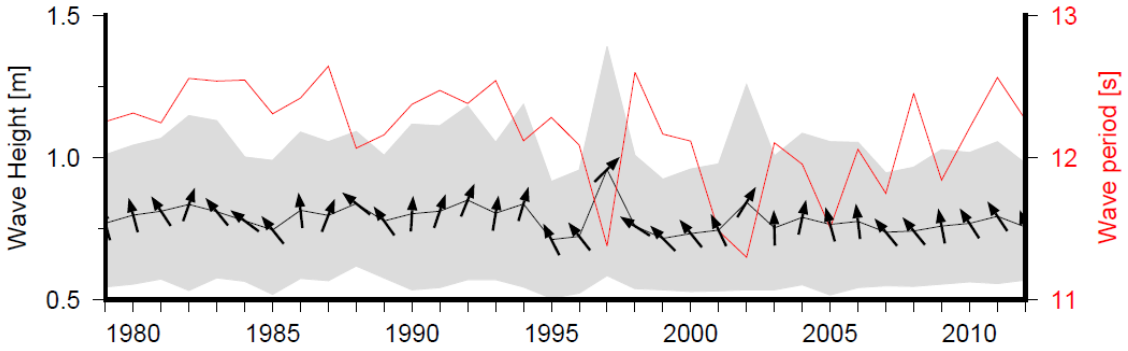

Figure 10: Annual wave conditions in Betio modelled by Bosserelle et al. 2015. The black line indicates wave height, red line illustrates wave period, and arrows indicate wave direction. Changes in pattern can be noted during the 1997–1998 El Niño event, which resulted in an increase in wave height, changes in wave direction, and a minimal wave period.

The prevailing wind for Tarawa is from the northeast with a mean speed of 5.01 m/s from 86° (Bosserelle et al. 2015).

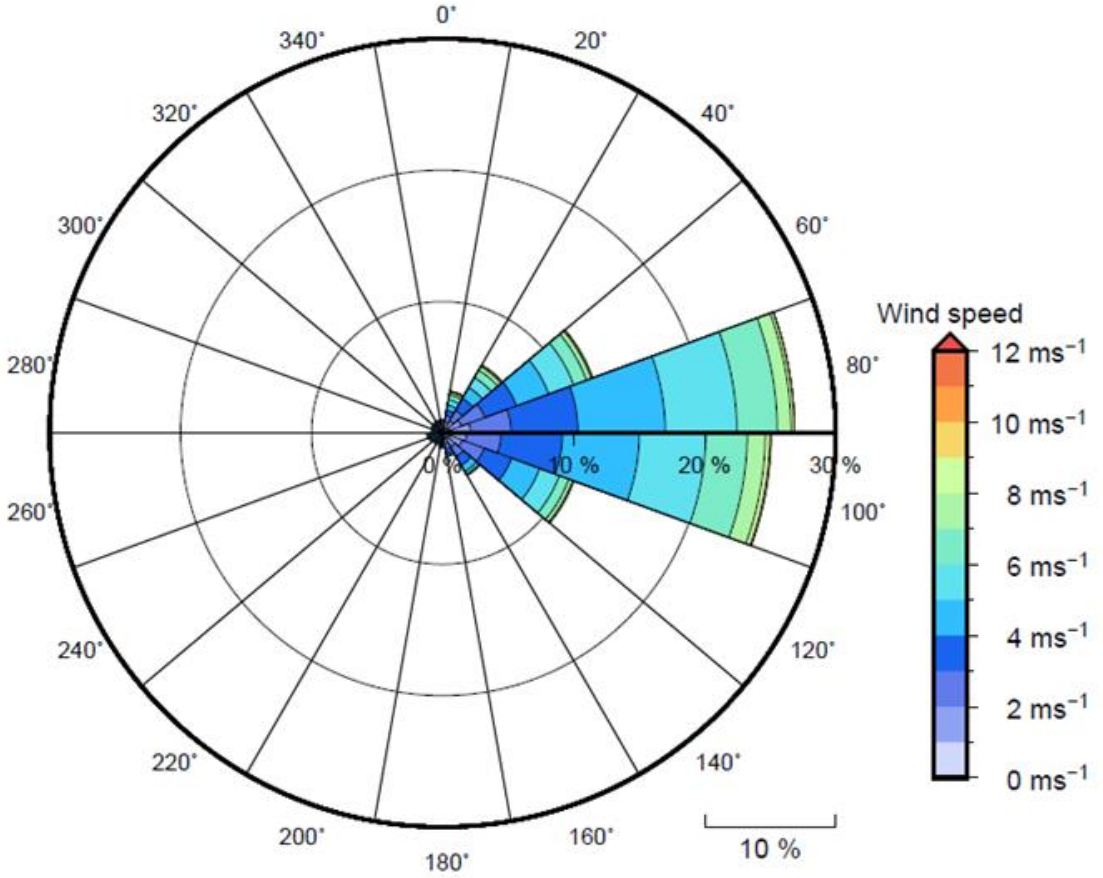

Figure 11: Wind rose for Betio, Tarawa Atoll. Adapted from Bosserelle et al. 2015. Directions use nautical convention (i.e. directions indicate where the wind is coming from).

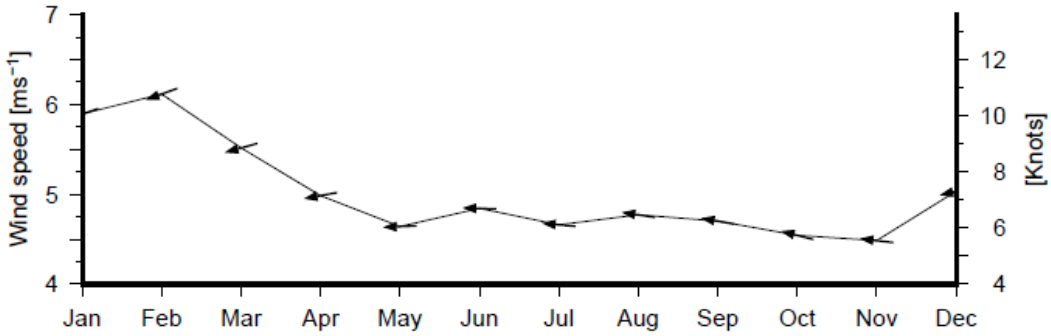

Figure 12: Monthly wind speed (black line) and wind directions (arrow). The main wind direction is from the northeast. Source: Bosserelle et al. 2015

2.3 Extreme water level analysis

A tide gauge in Betio permanently records surface elevation data. Data are available through the South Pacific sea level and monitoring project (http://www.psmsl.org/data/obtaining/stations/1739.php).

Figure 13 to Figure 18 show the results of a harmonic analysis from 22 years of tide data from the Betio tide gauge. The tidal planes were derived for Betio, calculated from the tidal constituents determined in the analysis.

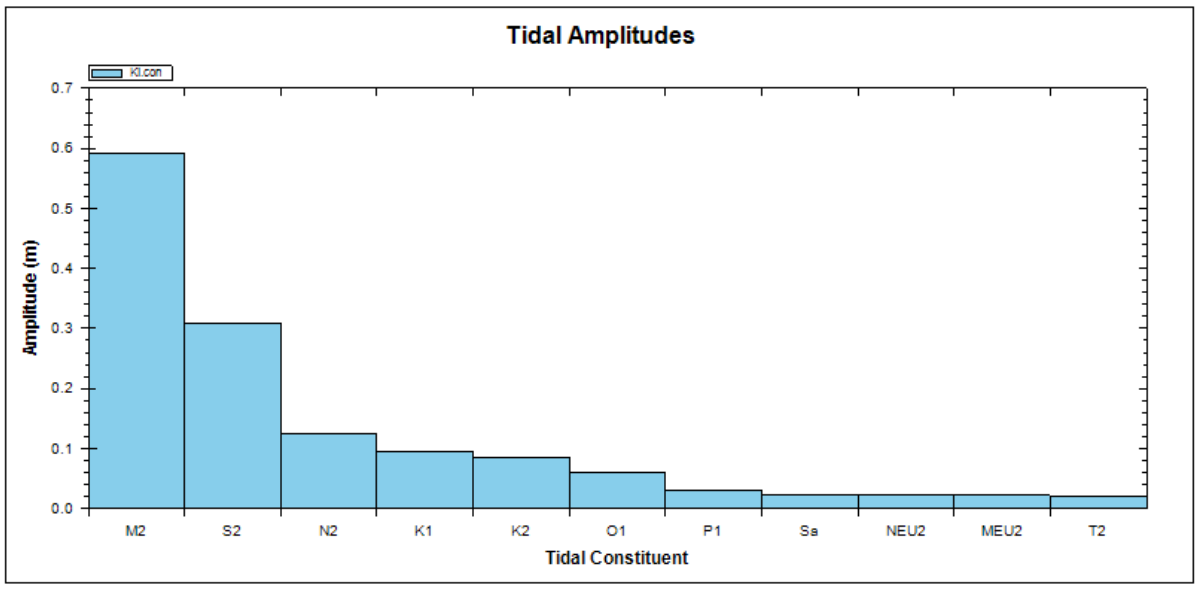

Figure 13: Output of harmonic constituents from tidal analysis. M2 = principal lunar semidiurnal constituent; S2 = principal solar semidiurnal constituent; N2 = larger lunar elliptic semidiurnal constituent; K1 = lunar diurnal constituent; K2 = lunisolar semidiurnal constituent; O1 = lunar diurnal constituent; P1 = solar diurnal constituent; Sa = solar annual constituent; NEU2 = larger lunar evectional constituent; MEU2 = variational constituent; and T2 = larger solar elliptic constituent.

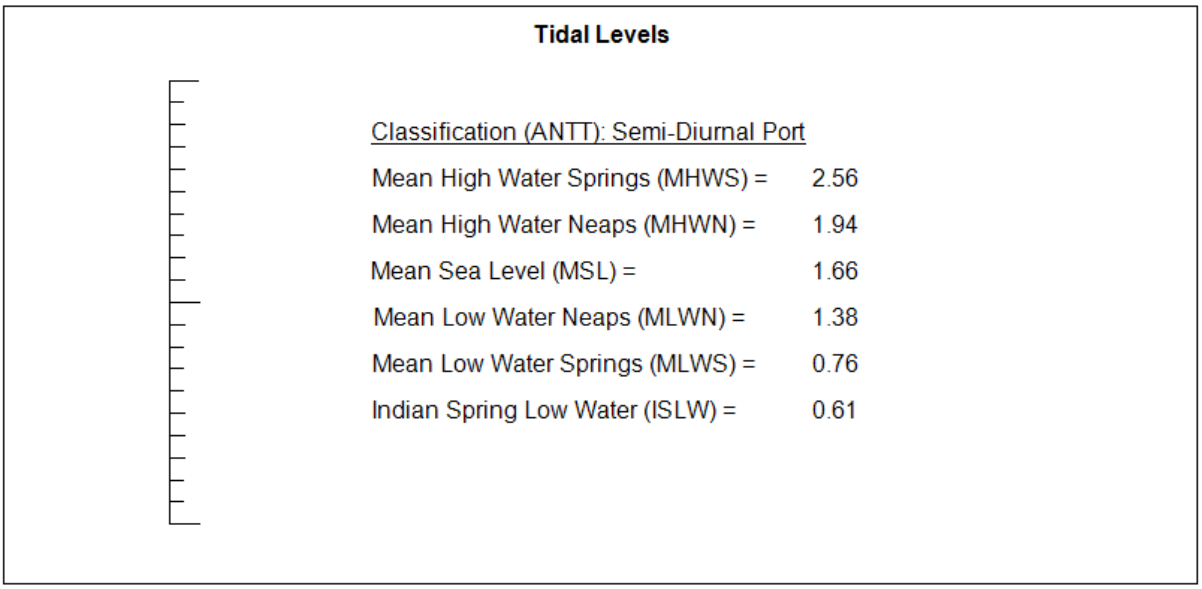

Figure 14: The tidal levels were derived based on the definition from the Australian Tides Manual. The definition of mean sea level is the arithmetic mean of hourly heights of the sea at the tidal station observed over a period of time, 22 years in this case.

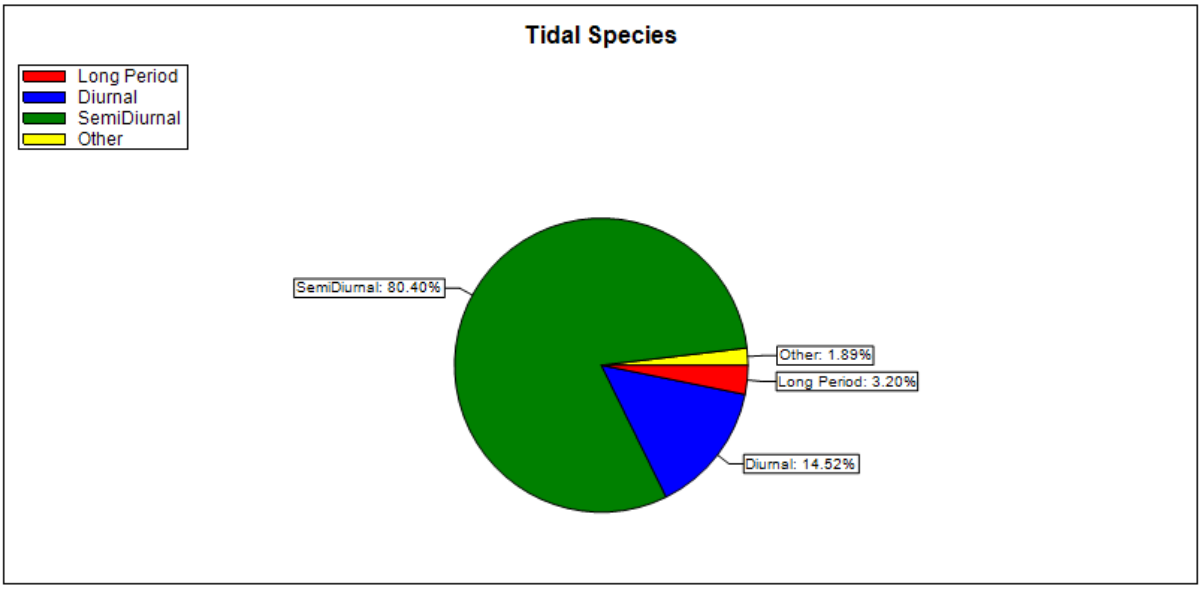

Figure 15: Analysis produced three major tidal species: long-period, diurnal and semidiurnal. Each tidal species contains groups of harmonics that can be separated by analysis of a month or year of observations

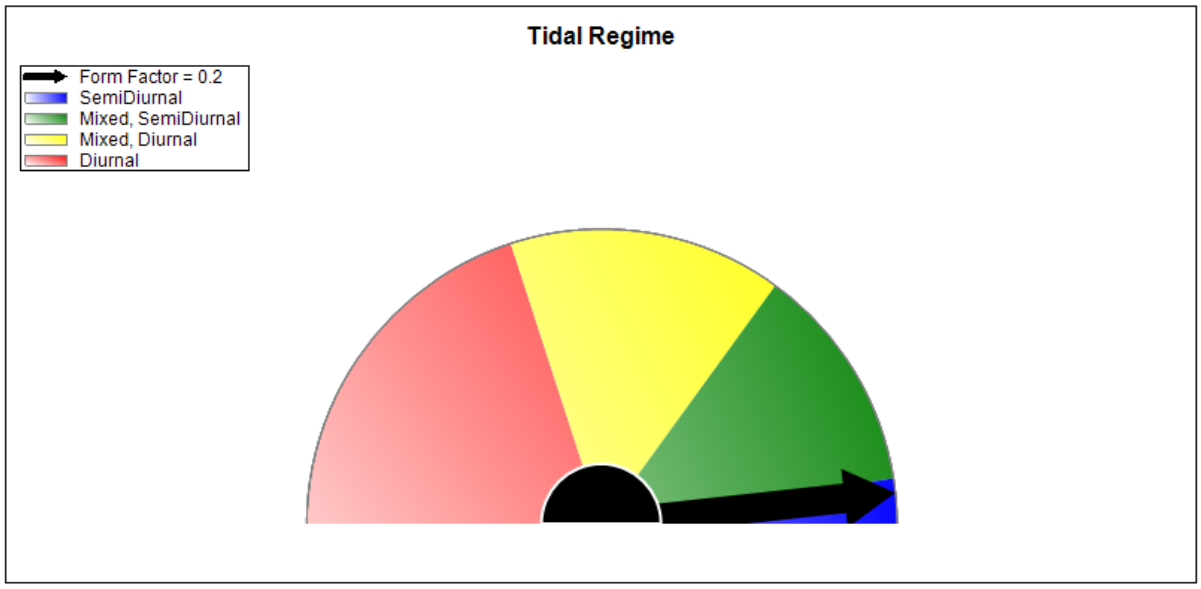

Figure 16: Tidal regime derived from long-term data show semidiurnal tides for Betio, Tarawa Atoll. This means that there are two tide cycles in a day — two highs and two lows — and that the two highs and two lows portray similarities in their heights.

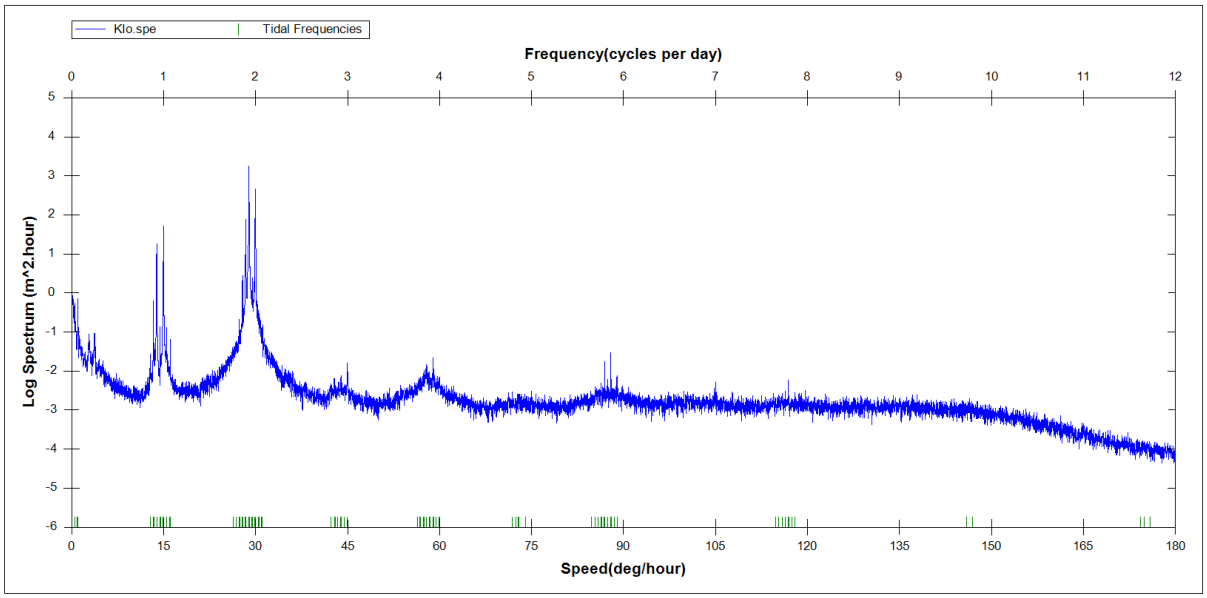

Figure 17: Plot of the spectrum of tides produced from harmonic analysis of 22 years of tide data.

Harmonic analysis on a long historical record of high quality observations takes into account the 18.6-year cyclic period (lunar ascending node) of tides. The constituents derived symbolise tide conditions for the Betio region.

The form factor was noted to be 0.2 (Figure 16) with a tidal range of 1.80 m. The mean sea level was derived to be 1.66 m and the major tidal species for Betio was found to be semidiurnal, which indicates that Betio has two highs and two low tides in a day with almost the same height. Figure 17 shows a plot of the spectrum of tides with frequencies near twice per day (semidiurnal tides). The monthly mean sea level variation range is 0.07 m with the largest variation recorded during the 1997–1998 El Niño event.

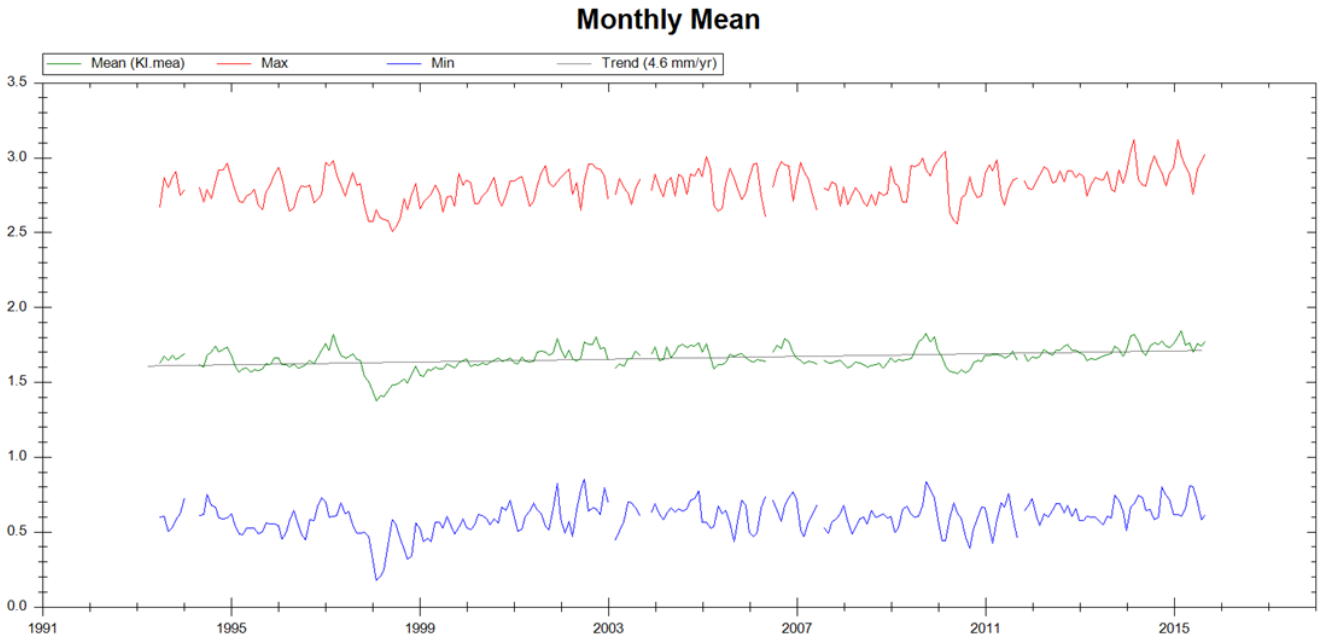

Figure 18: Maximum and minimum sea levels calculated on a monthly basis for each respective year. The linear trend of sea level was derived to be 4.6 mm per year.

From the 22 years of data, the maximum recorded sea level was on 19 February 2015 at 05:00 and the minimum recorded sea level was on 26 February 1998 at 11:00. The maximum value was 3.120 m whereas the minimum value was 0.175 m. The lowest value recorded could be attributed to atmospheric conditions as on 26 February 1998; a total solar eclipse occurred, with corresponding spring tides, which coupled with the El Niño event of 1997–1998 resulted in a larger tidal variation, thereby resulting in a very low tide. The maximum value recorded on 19 February 2015 is attributed to extreme events occurring weeks before Tropical Cyclone Pam hit the region.

Extreme distribution analysis for Tarawa was completed by Damlamian et al. (2015). Analysis was performed for the total water level, the water level corrected from mean sea level anomaly and the storm surge. The analysis was performed using a peak-over-threshold approach and by fitting a generalised Pareto distribution (GDP) to the peaks. The thresholds were selected based on the shape parameter of the distribution, the threshold stability property and sensitivity of the 100-year return value. The 95% confidence interval was also calculated for each distribution. The extreme value analysis, threshold selection, and confidence calculation were performed using the ORCA package (Deltares, 2012).

Table 2: Selected thresholds with the number of peaks for the extreme water level analysis. Source: Damlamian et al. 2015

	Selected threshold (m)	Number of peaks
Total water level	2.80 m above SEAFRAME datum	165
Corrected water level	2.88 m above SEAFRAME datum	104
Storm surge	0.06 m above mean sea level	39

The amplitudes of constituents M2, S2 and N2 are used to derive the mean high water perigean spring high tide commonly as ‘king tides’. The tidal level (1.03 m) (Table 3) is exceeded by 8% of high tides. The mean high water spring (spring high tides) is derived from the combined amplitude of the M2 and S2 tidal harmonics (0.9 m) with the mean high water

calculated as an average elevation of high tide. MHWS is exceeded by 19% of high tides. MHWN is the difference in amplitude of M2 and S2 tidal harmonics level of the tide (0.28) exceeded by 90% of high tides.

Table 3: Mean values calculated from tidal constituents produced by the harmonic analysis. These values are adjusted to mean sea level. Source: Damlamian et al. 2015

	Mean high water perigean pring (MHWPS)	**Mean high water spring (MHWS)**	**Mean high water (MHW)**	**Mean high water neap (MHWN)**
Values are in meters above mean sea level	1.03	0.9	0.65	0.28

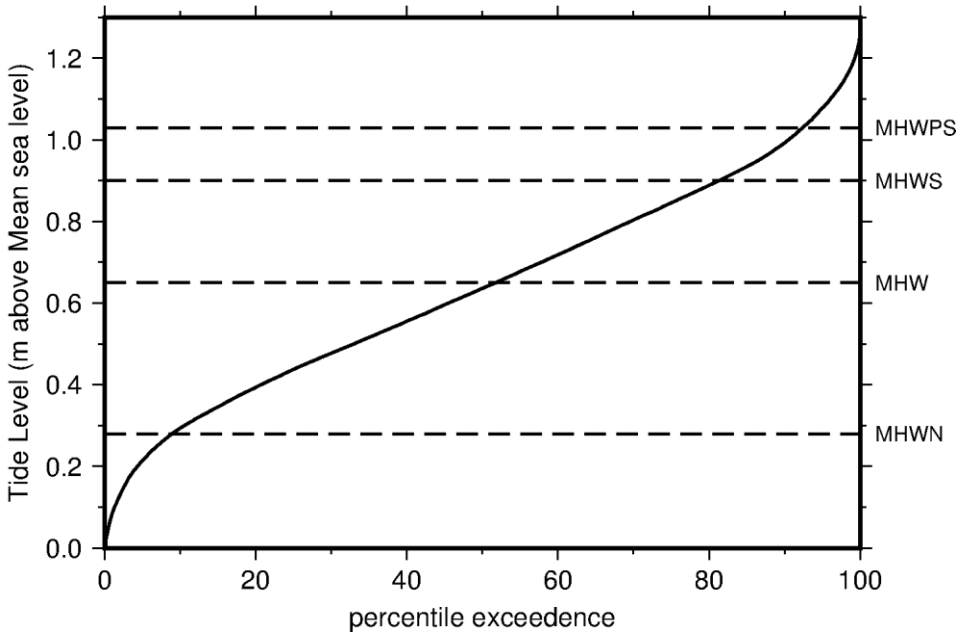

Figure 19: Tidal exceedance curve. Source: Damlamian et al. 2015

Extreme distribution of water level was completed directly on the total water level measured by the Sea-level Fine Resolution Acoustic Measuring Equipment (SEAFRAME) tide gauge. The extreme distribution fitted to the peaks above the threshold level and the 100-year return value is 2.04 m above the SEAFRAME reference datum, Table 4, (**Error! Reference source not found.**).

The total water level includes the tide, storm surges, and the variation in the mean water level. Monthly variation of the mean water level can be 0.22 m and persist for several months. Therefore, the mean sea level variation can exaggerate or hide high water level due to the co-occurrence of spring tides and storm surge. To get a more representative picture of the return values for water level due to the co-occurrence of just tide and storm surge, the extreme distribution analysis was done on the total water level with the monthly mean sea level removed (Figure 18). This corresponds to the contribution of tide and storm surges. The extreme distribution of the tide and storm surge shows a shape parameter closer to zero. This results in a 100-year return value of 2.07 m, Table 4. An extreme distribution was fitted to the

storm surge data (Figure 20), the 100-year return value was found to be 0.13 m above mean sea level, Table 4: Water level and storm surge return values calculated for 10, 20, 50 and 100 years. **Source: Damlamian et al. 2015**(**Error! Reference source not found.**).

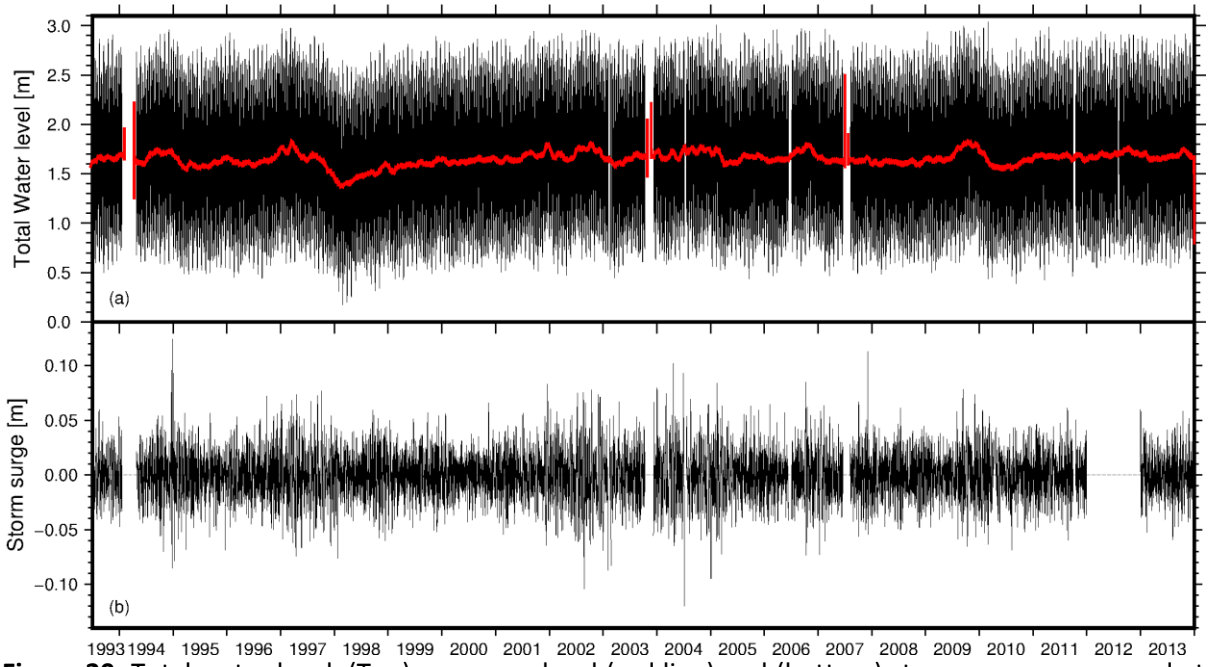

Figure 20: Total water level. (Top) mean sea level (red line) and (bottom) storm surges measured at Betio between 1993 and 2013. Source: Damlamian et al. 2015

Table 4: Water level and storm surge return values calculated for 10, 20, 50 and 100 years. Source: Damlamian et al. 2015

Return period (year)	Storm surge return value (m)	Total water level return value (m above SEAFRAME)	Tide +storm surge return value (m above SEAFRAME)
10	0.10	2.01	2.03
20	0.11	2.02	2.05
50	0.12	2.03	2.06
100	0.13	2.04	2.07

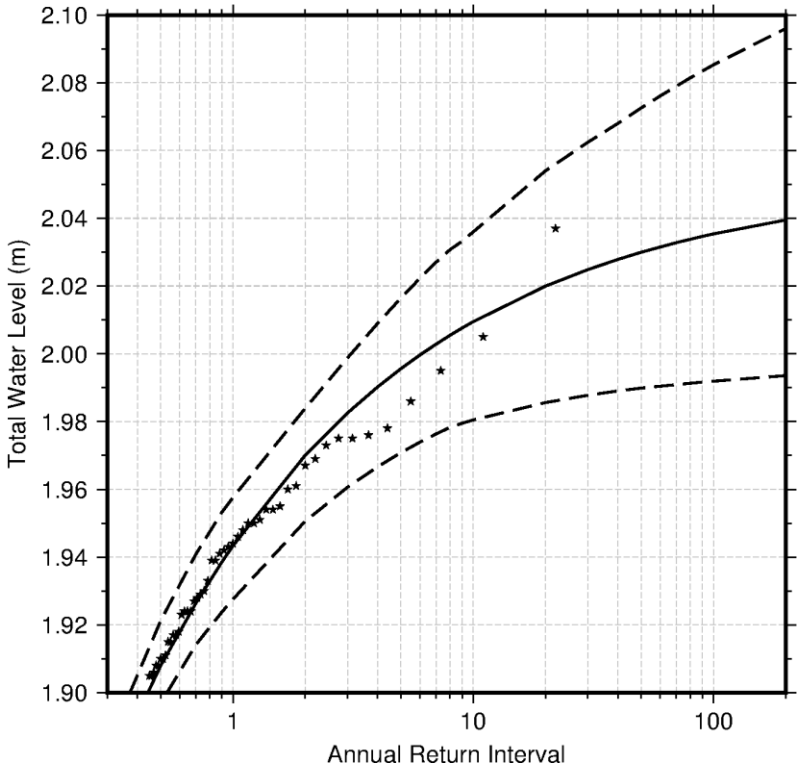

Figure 21: Extreme value distribution of total water level. Data are represented by stars, the black line shows the best fit to the extreme values, and dashed lines indicate the 95% confidence lines of the fit. Source: Damlamian et al. 2015

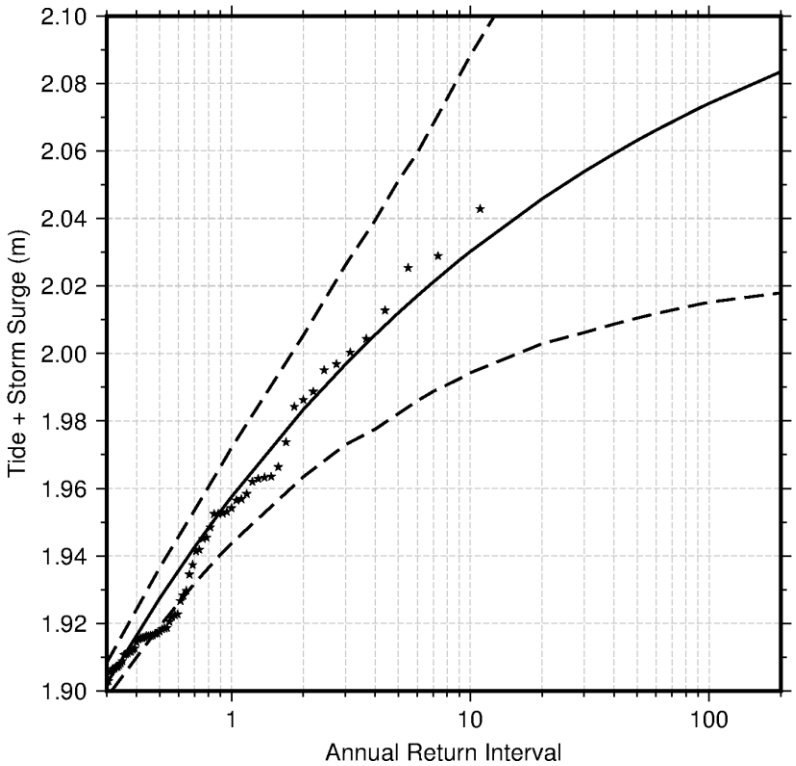

Figure 22: Extreme value distribution of storm surge. Data are represented by stars, the black line shows the best fit to the extreme values, and dashed lines indicate the 95% confidence lines of the fit. Source: Damlamian et al. 2015

2.4 Offshore bathymetry

The offshore bathymetry for Tarawa was conducted during the European Union Development Fund 8/9 project by Kruger et al. (2007). The datasets are set at the drop of the reef slope with a minimum depth of 50–10 m and a maximum depth of 1,300 m. The area covered was 3 km all around Tarawa.

Another survey was completed by RV *Melville* in 1999, which covers some areas of Tarawa.

Data are also available via global bathymetry datasets. Global data for Kiribati merge the satellite altimeter data derived by Smith and Sandwell (1997) with, General Bathymetric Chart of the Oceans GEBCO over shallow depths (Marks and Smith 2006).

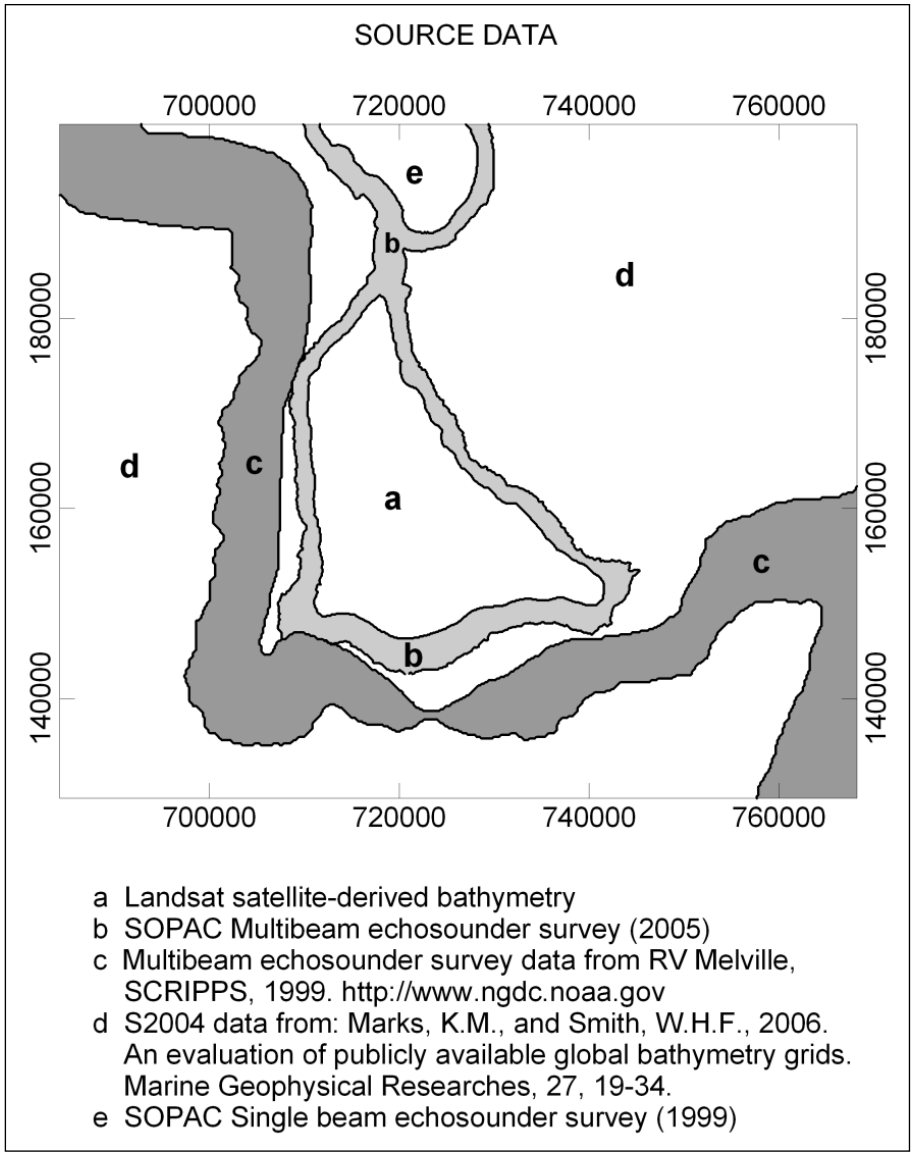

Figure 23: Available bathymetry data sources and coverage for Tarawa, Kiribati. Source: Kruger et al. 2008

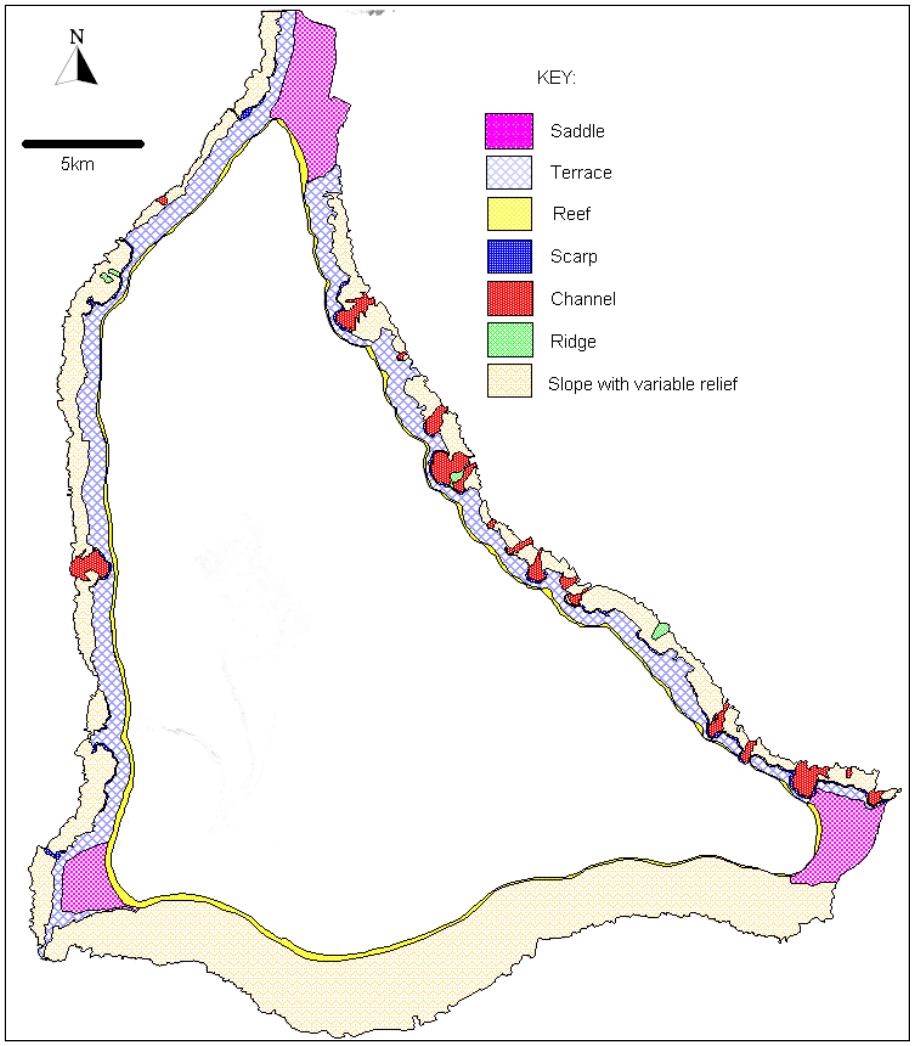

Figure 24: Morphological features of Tarawa Atoll interpreted by Kruger et al. 2008

Table 5: A summary of submarine morphology for Tarawa Atoll. Adapted from Kruger et al. 2008.

Depth	Feature
~40 m	**Reef platform, up to 100 m wide**
~50 m	**Seaward sloping seabed, 30–40^{o}**
250–450 m	**Numerous seaward convex scarps, slope angle 40–60^{o}. Submarine ridges on all three ends of the triangle shape of Tarawa, the northern ridge at ~300 m depth is 2.5 km wide connecting to Abaiang, the southwest ridge at 250 m depth is 2 km wide and the south eastern ridge also at 250 m depth is 2.5 km wide.**
500–1,500 m	**Variable relief including scarps, canyons, and channels. Slope angle 30–60^{o}**

Table 6: Reference system adopted by Kruger et al. (2008) for the bathymetry survey.

Geodetic datum	WGS84	
Ellipsoid	WGS84	
	semi-major axis (a)	6378137.000
	semi-major axis (b)	6356752.314
	inverse flattening (1/f)	298.257223563
	eccentricity sq. (e^2)	0.0066943800
Projection	UTM Zone 59 North	
	projection type	Transverse Mercator
	origin latitude	00° 00' 00.000" North
	origin longitude	171° 00' 00.000" East
	origin false easting	500 000.000
	origin false northing	0.000
	Scale factor	0.9996000000
	grid unit	metres
Geodetic transformation	from WGS84 (GPS satellite datum) to UTM 59N	
	source coordinate system	WGS84
	target coordinate system	UTM 59N
	transformation parameters	
	dX	0.00
	dY	0.00
	dZ	0.00
	rX	0.00000
	rY	0.00000
	rZ	0.00000
	scale	0.00000

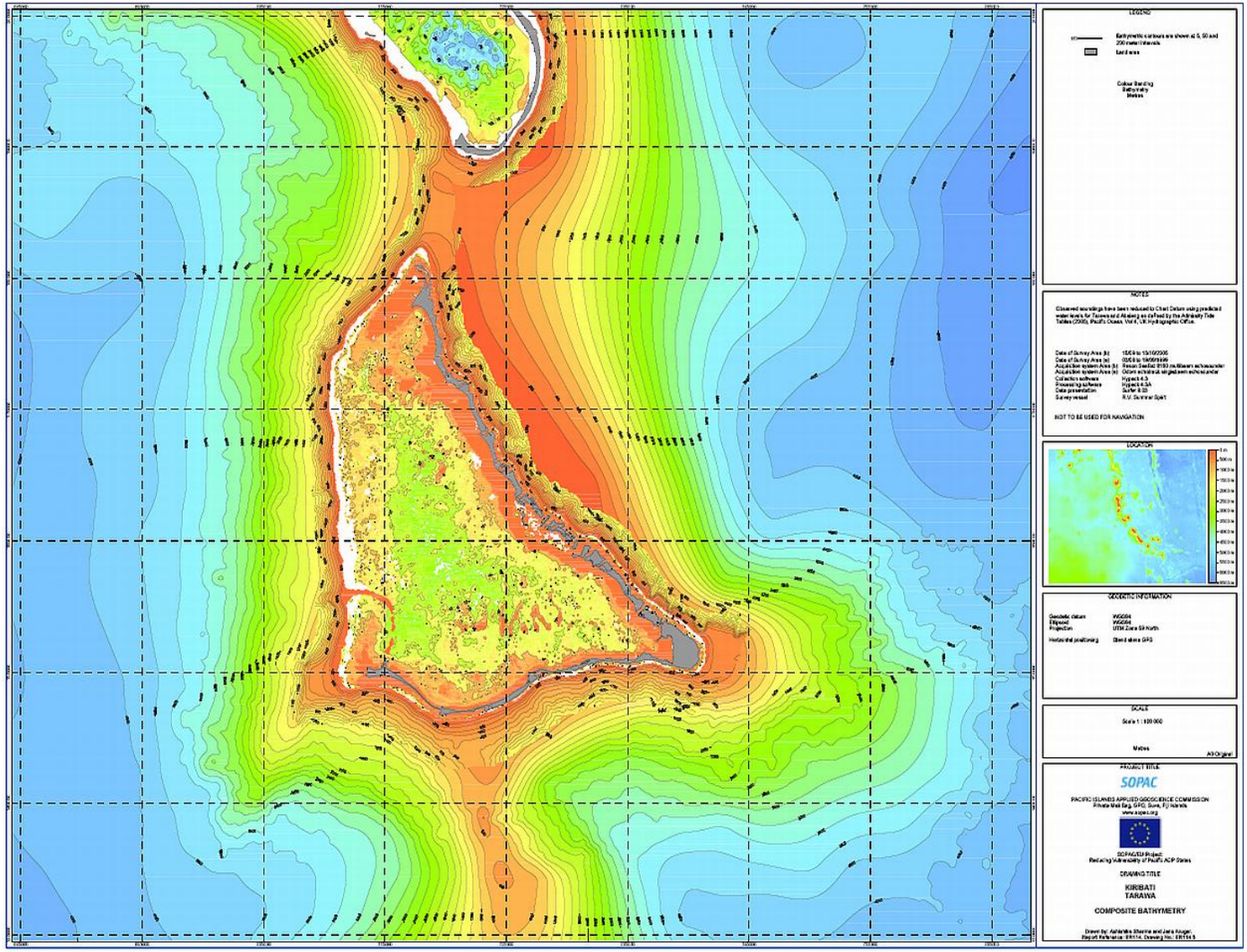

Figure 25: Bathymetry chart of Tarawa Atoll produced by Kruger et al. (2008)

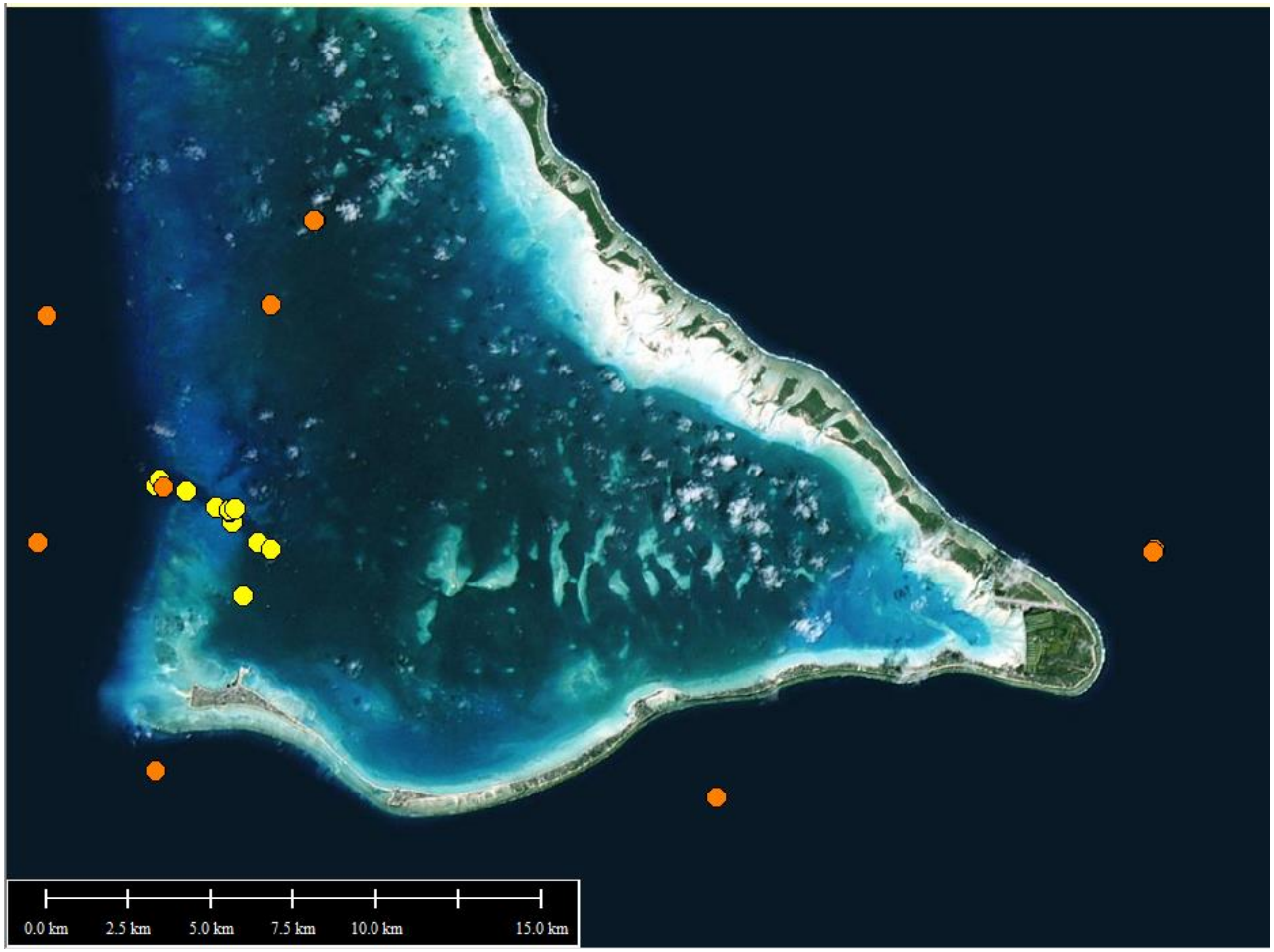

Figure 26: Locations of conductivity, temperature and depth cast during the survey by Kruger et al. (2008) (yellow), and Kumar et al. (2015) (orange),

2.5 Argo floats

Argo floats were initiated through an international collaboration to acquire high quality temperature and salinity profiles from water depths down to 2000 m. In total, 51 stations close to Tarawa waters were selected.

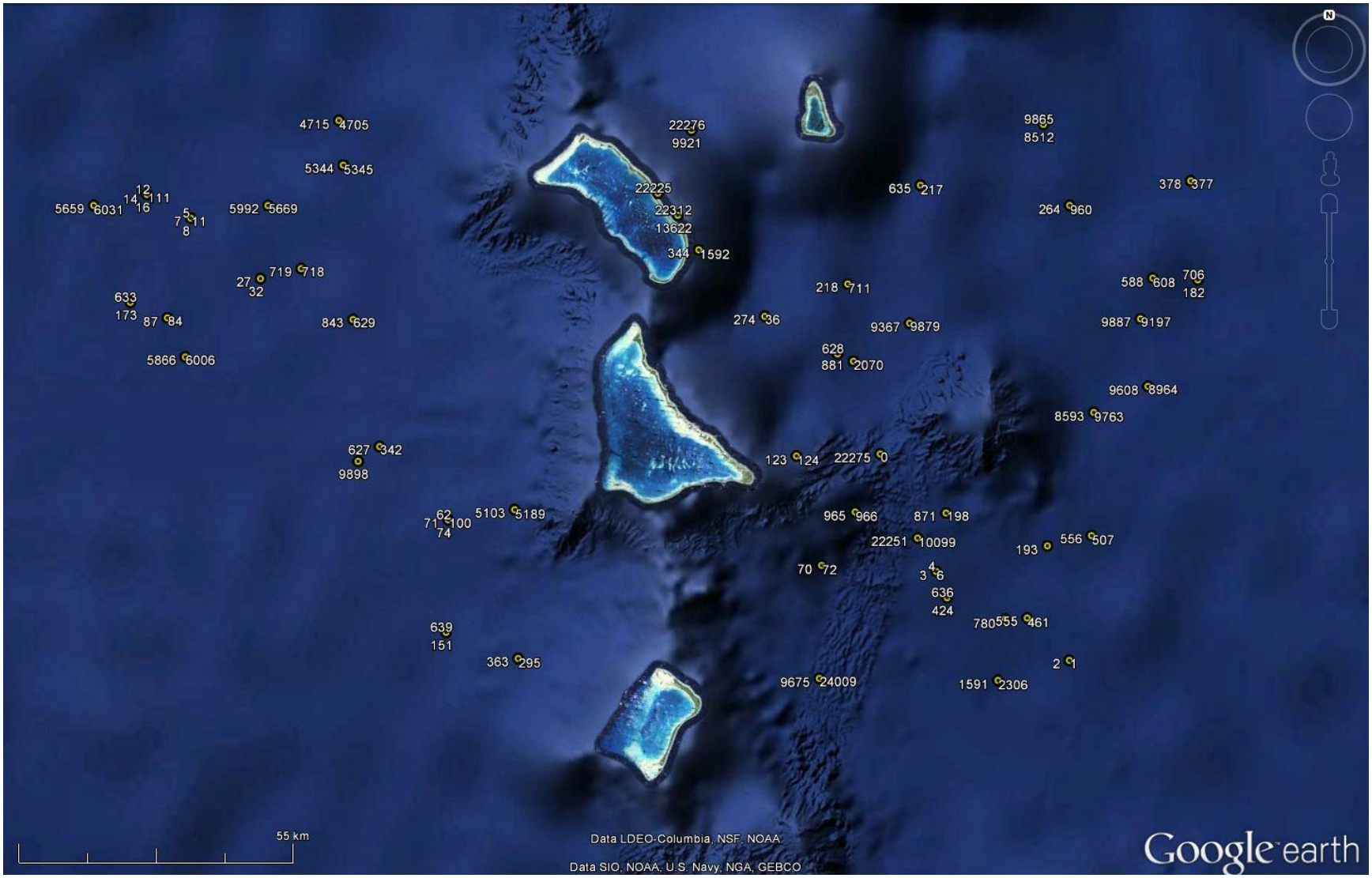

Figure 27: Argo float station locations for Tarawa waters plotted on a Google backdrop.

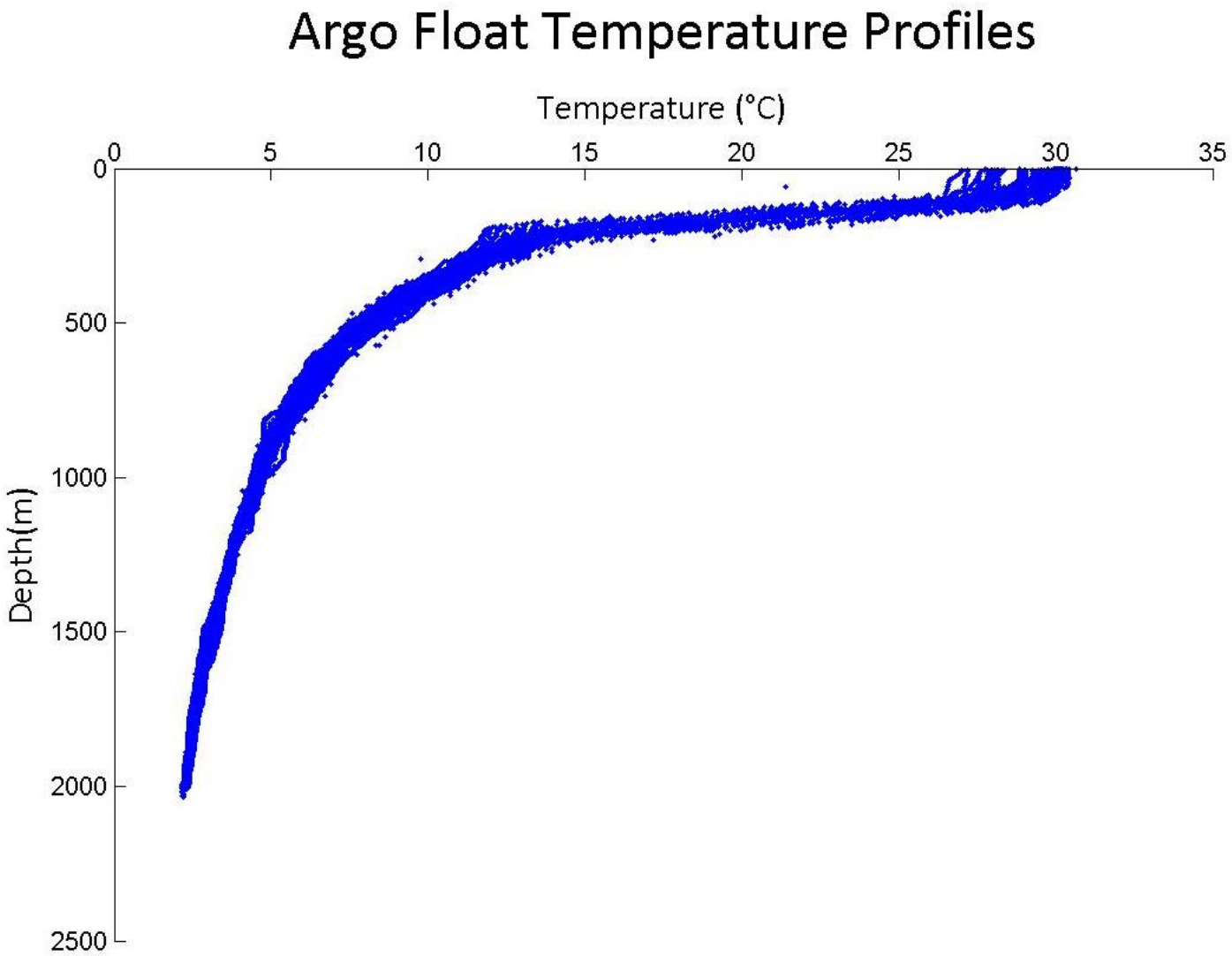

Figure 28: Temperature profiles extracted from the 51 Argo stations in Tarawa waters.

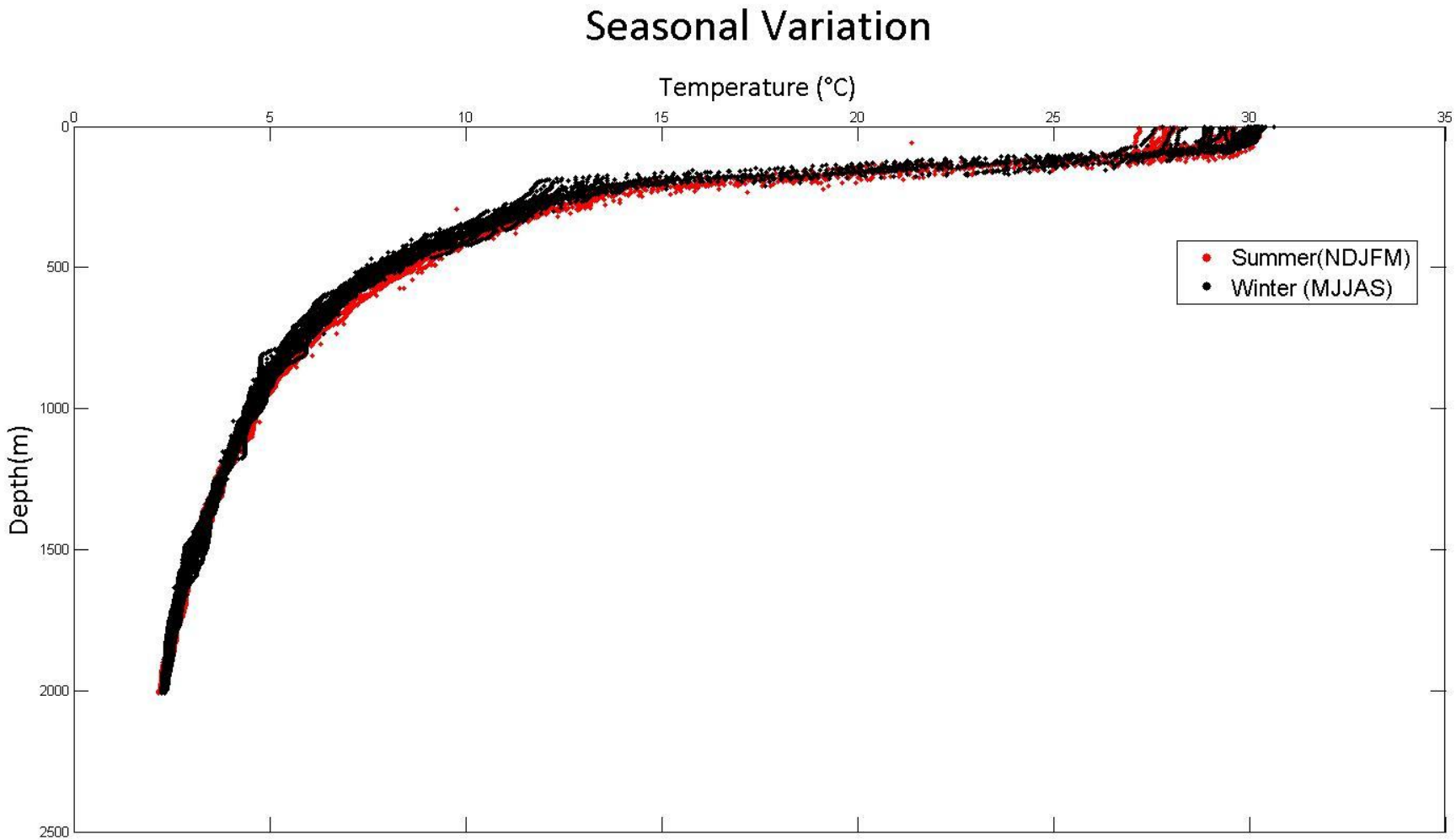

Figure 29: Temperature data plotted according to two seasons, summer and winter. Winter includes the months of May, June, July, August and September, whereas summer consists of November, December, January, February and March.

Table 7: Temperature statistics for summer and winter seasons. The aim was to evaluate seasonal variation in temperature for a respective depth.

Depth (50 m)	**Temperature**	**Summer (S1)**	**Winter (S2)**	**Variation (S1-S2)**
	Minimum	21.38	26.98	-5.60
	Maximum	30.25	30.25	0.00
	Mean	29.02	29.47	-0.45
	Standard deviation	1.03	0.66	0.37
Depth (250 m)	**Temperature**	**Summer**	**Winter**	
	Minimum	12.89	11.69	1.20
	Maximum	21.69	21.48	0.21
	Mean	16.53	14.58	1.95
	Standard deviation	2.06	1.91	0.15
Depth (500 m)	**Temperature**	**Summer**	**Winter**	
	Minimum	7.07	6.80	0.27
	Maximum	8.43	7.72	0.71
	Mean	7.54	7.26	0.28
	Standard deviation	0.30	0.22	0.08
Depth (750 m)	**Temperature**	**Summer**	**Winter**	
	Minimum	5.38	5.30	0.08
	Maximum	6.70	6.38	0.33
	Mean	5.89	5.69	0.20
	Standard deviation	0.23	0.23	0.00
Depths (1,000 m)	**Temperature**	**Summer**	**Winter**	
	Minimum	4.42	4.34	0.08
	Maximum	4.83	4.89	-0.07
	Mean	4.61	4.58	0.03
	Standard deviation	0.09	0.15	-0.06
Depth (1,250 m)	**Temperature**	**Summer**	**Winter**	
	Minimum	3.70	3.74	-0.04
	Maximum	4.12	4.29	-0.17
	Mean	3.90	3.90	-0.01
	Standard deviation	0.07	0.09	-0.02

The Argos data collated from 51 stations revealed no significant variation in temperature plotted against depth.

Figure 28, shows the trend of temperature with depth, which is similar for all 51 stations. The thermocline depth interpreted from the plot seems to be the same for all profiles.

For a rigorous comparison, data were extracted based on seasons, November to March as summer and May to September as winter. Seasonal data (

Figure 28 show very little variation in temperature. Because the data ranged from 2004 to early 2015, no comparison was made for any ENSO events. The La Niña event of 2010–2011 did not have much impact on SST, and was globally classified as a moderate event.

Figures 29 shows temperature statistics analysed for various depths. The minimum, maximum, mean, and standard deviation was calculated at the same depth for the two different seasons. A temperature analysis for the two seasons revealed little or almost no variation for most depths. Table 7 shows a general decreasing trend of variation along the profile depth.

2.6 Field survey

Two field surveys were completed as part of the OTEC feasibility study. The first trip was in August 2015 and the second was in November 2015. Field surveys included measuring temperature and salinity for depths up to 1,200 m. These measurements were taken in the three locations identified by the Korean Research Institute of Ships and Ocean Engineering (KRISO) as in Figure 30. Furthermore, meetings were held with the Ministry of Works and the Ministry of Environment in Tarawa regarding the next phase of the project.

Figure 30: Setting the winch system on the survey boat. A dual frequency echo sounder, purchased by the Korean Research Institute of Ships and Ocean Engineering, was mounted on the starboard side of the boat.

The main objective was to cast a CTD (conductivity, temperature and depth) instrument (Figure 31) to depths of up to 1,000 m. The echo sounder mounted by KRISO was supposed to survey transects and create depth profiles from the reef edge to the CTD sampling point of 1,000 m.

Problems were encountered with the echo sounder, however, so the survey team opted to use bathymetry data from Kruger et al. (2008). The second objective was to conduct sediment sampling from depths of 500 m, 750 m, 1,000 and 1,200 m using a gravity corer (see Figure 32).

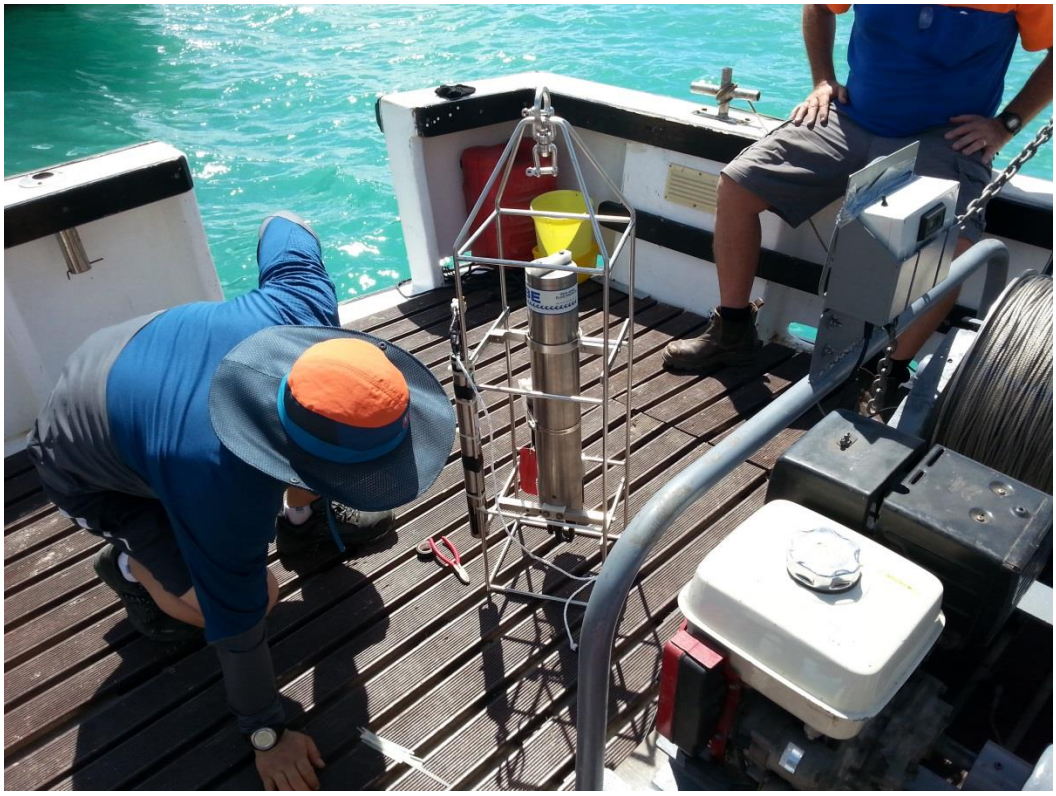

Figure 31: Conductivity, temperature and depth (CTD) instrument ready to be deployed. A separate CTD from the Korean Research Institute of Ships and Ocean Engineering was mounted with the Geoscience Division CTD, which was deployed using a winch.

Figure 32: Geoscience Division technical staff deploying the gravity corer to depths of ~1,000 m. The launch was controlled using the winch motor break and released in free fall when the corer was ~30 m above the sea bed.

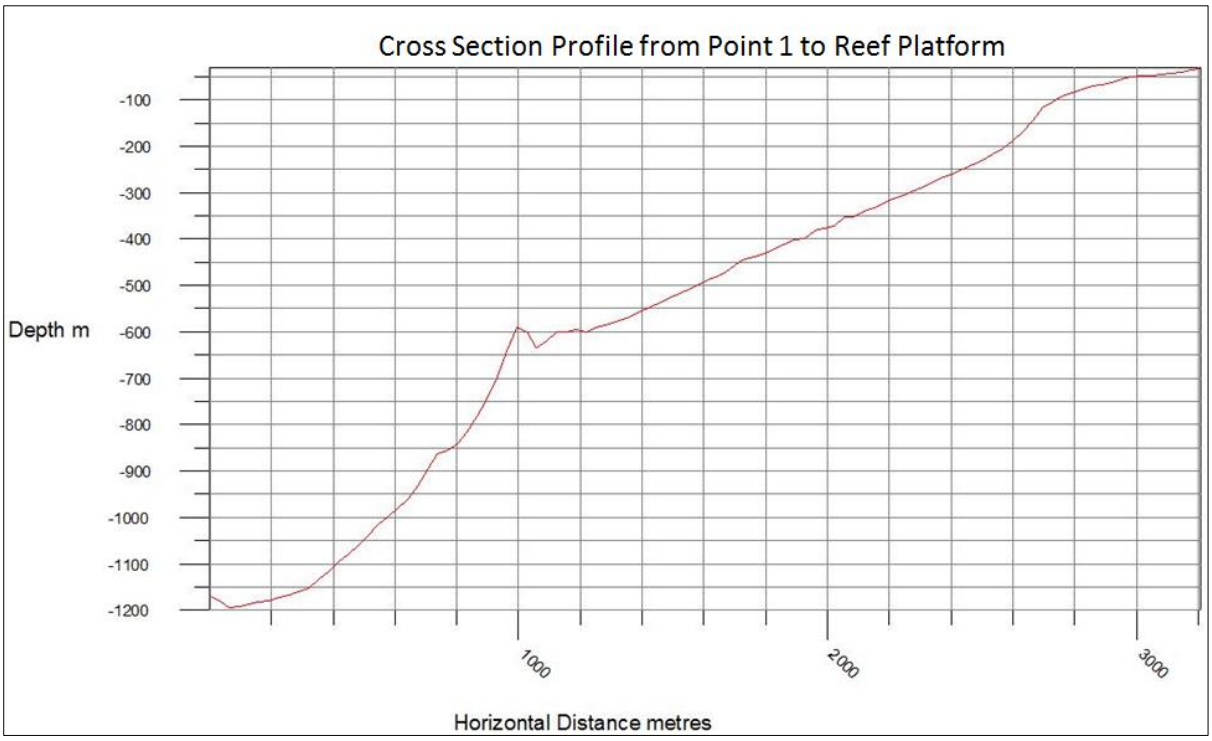

Figure 33: Cross section profile derived from bathymetry data (Kruger et al. 2008). Profile shows seabed morphology from Point 1 to the reef platform.

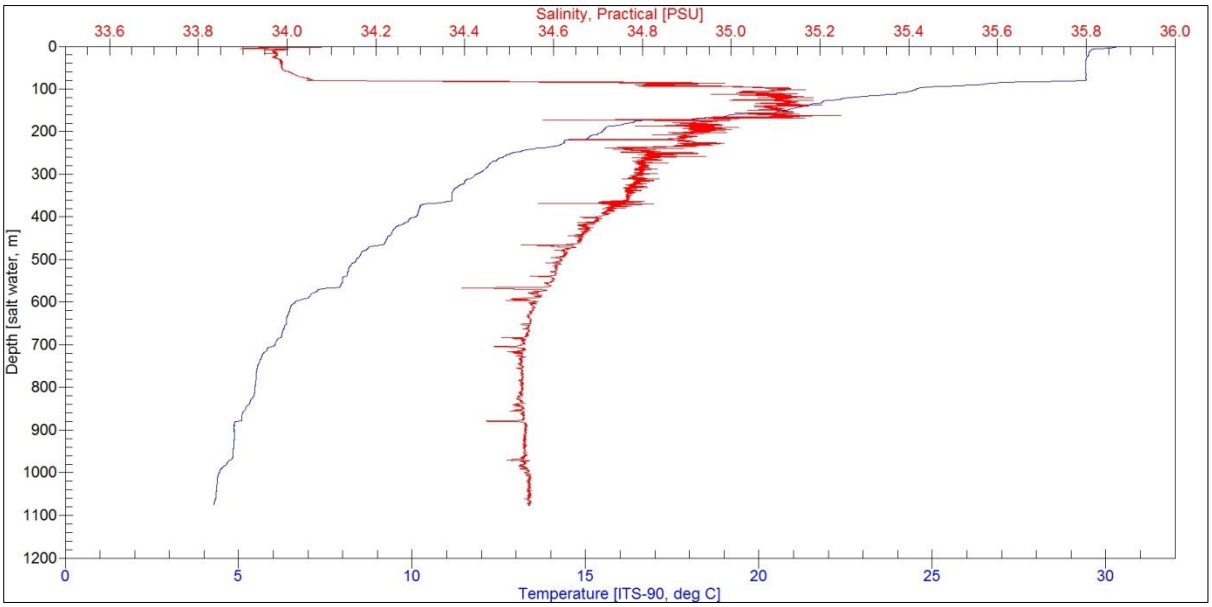

Figure 34: Conductivity, temperature and depth data from Point 1 showing temperature (blue) and salinity (red) to a depth of 1,076.6 m. The temperature at the maximum depth was 4.28°C.

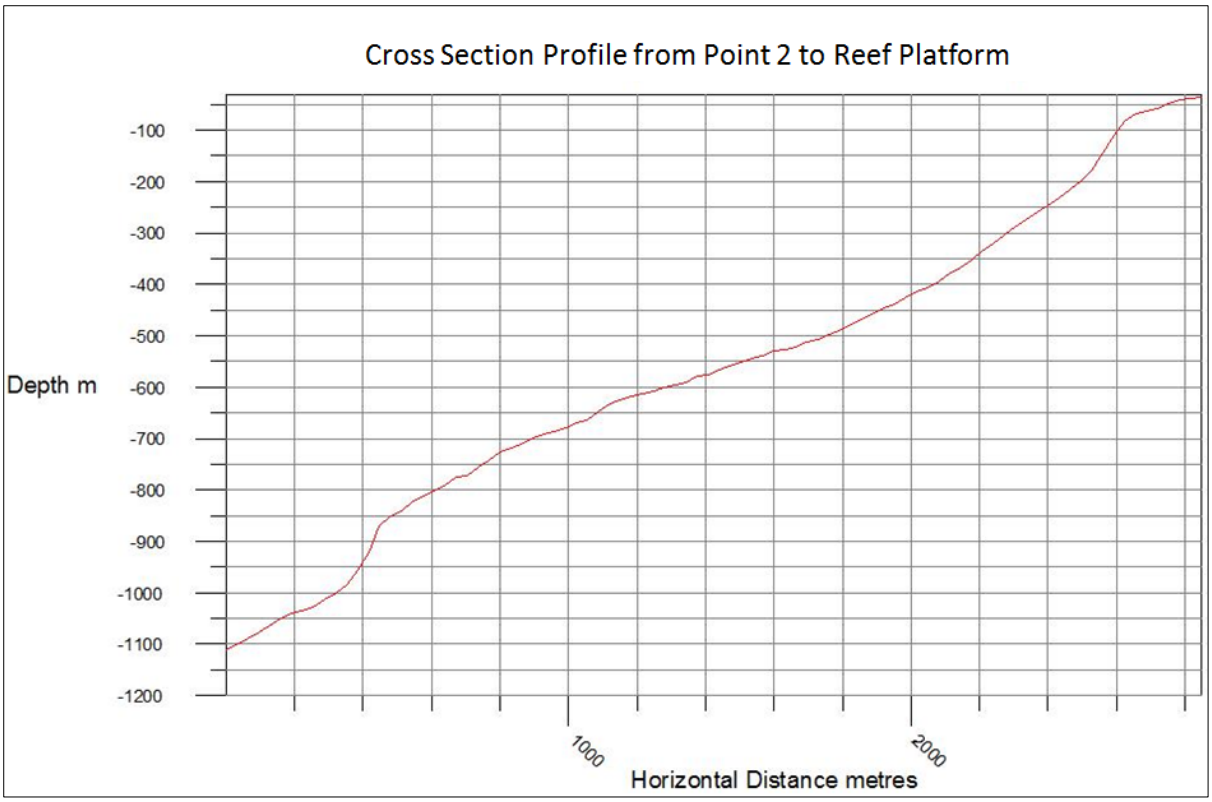

Figure 35: Cross section profile derived from bathymetry data (Kruger et al. 2008). Profile shows seabed morphology from Point 2 to reef platform.

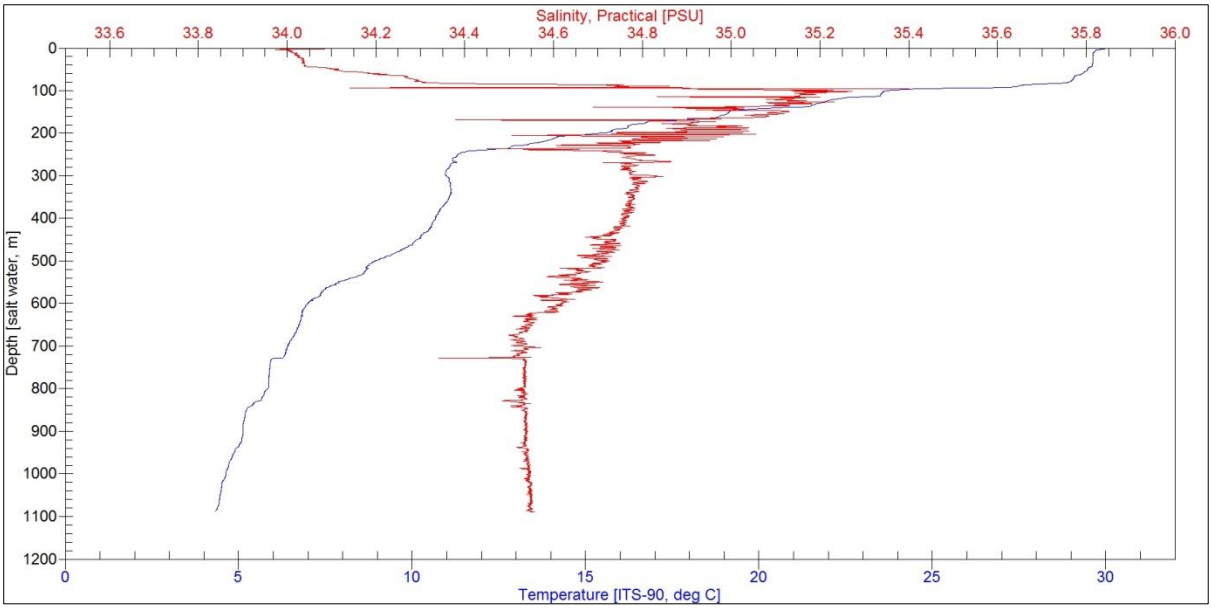

Figure 36: Conductivity, temperature and depth data from Point 2 showing temperature (blue) and salinity (red) to a depth of 1,089.5 m. The temperature at the maximum depth was 4.32°C.

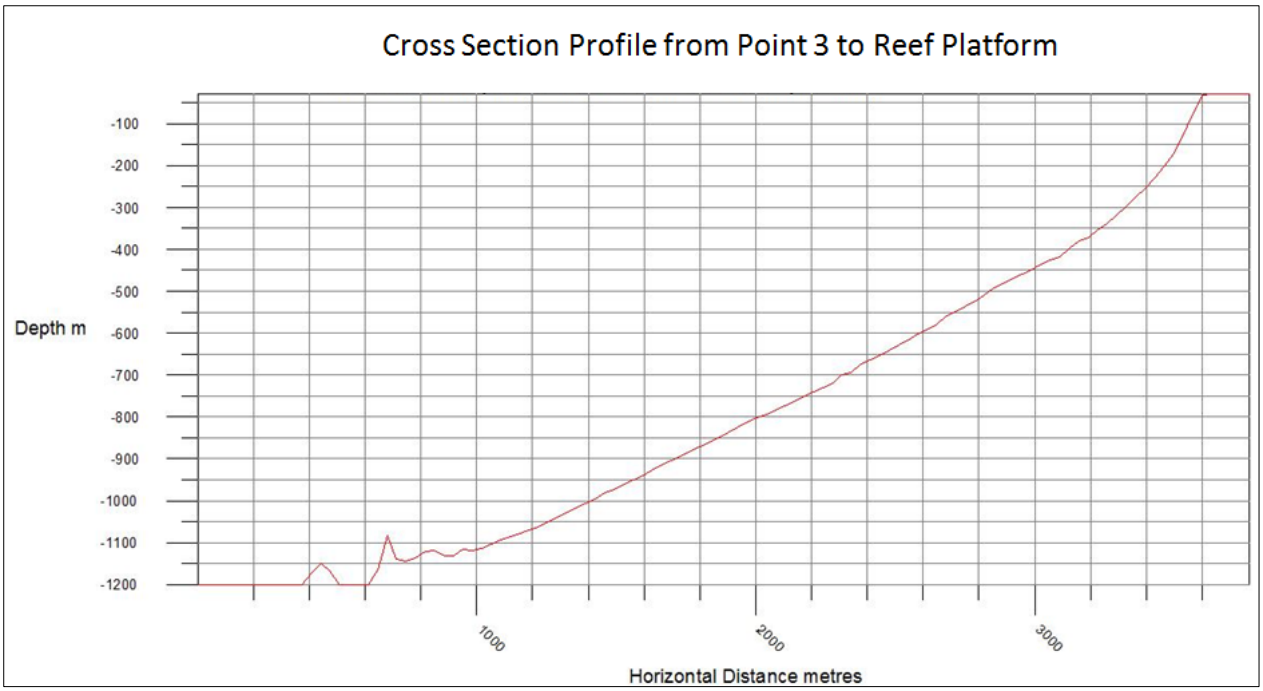

Figure 37: Cross section profile derived from bathymetry data (Kruger et al. 2008). Profile shows seabed morphology from Point 3 to reef platform.

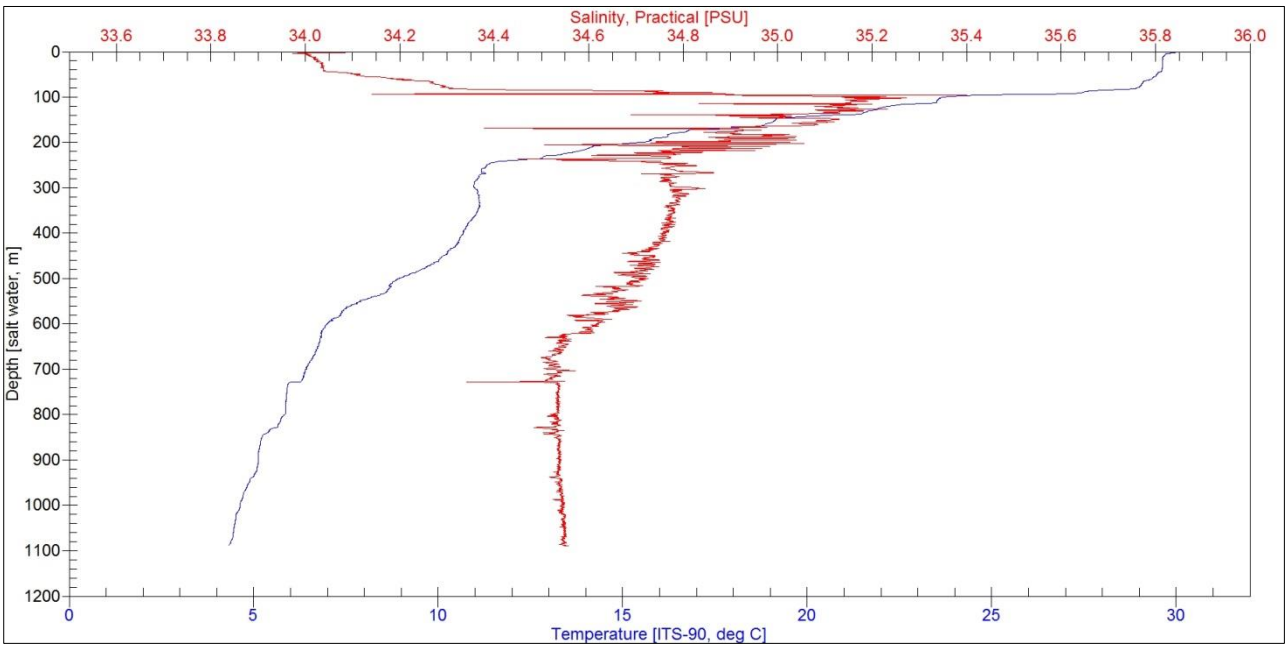

Figure 38: Conductivity, temperature and depth data from Point 3 showing temperature (blue) and salinity (red) to a depth of 1,089.5 m. The temperature at the maximum depth was 4.32°C.

3 Conclusion

This report describes the general oceanographic conditions and thermocline properties for South Tarawa, as part of the Preliminary Feasibility Study for Ocean Thermal Energy Conversion project, and combines phase 1 and phase 2 of the project (i.e. desktop study and field surveys).

Previous studies on the thermocline evolution with ENSO in the region were reviewed and the factors controlling thermocline depth was discussed. The thermocline structure has been defined by many authors using Sverdup dynamics, which is controlled by zonal wind stress and wind stress curl.

During La Niña events, the thermocline becomes deeper with a decrease in SST, whereas the thermocline becomes shallower during El Niño events, with an increase in temperature. This, however, was impossible to validate for Tarawa because the Argo data did not capture any of the ENSO event.

Oceanographic and water quality data were difficult to review because the related information was limited for the study sites on the ocean side of Tarawa. Most of the previous studies conducted for Tarawa were based on lagoon water. Extreme analysis for wind and wave were adopted from Bosserelle et al. (2015). The main directions and seasonal interaction and variation with ENSO events were highlighted.

An extreme water level analysis was completed using 22 years of data recorded from the tide gauge at Betio. A harmonic analysis was completed and 116 constituents produced which were used to derive the tidal conditions and regimes for Tarawa. The mean sea level was calculated to be 1.66m and the tidal species was found to be semidiurnal with a form factor of 0.2. Extreme analysis on water level was adopted from Damlamian et al. (2015). Thresholds were calculated using a peak-over-threshold approach, and levels for total water, corrected water level and storm surge were calculated.

Offshore bathymetry data for Tarawa was reviewed. The majority of the data was conducted during the European Union Development Fund 8/9 project by Kruger et al. (2008) and combined with datasets from RV *Melville* in 1999.

Argos data were downloaded from 51 stations. The datasets did not reveal any significant variation in temperature along profile depth. Argo profiles also did not capture any of the ENSO events, hence temperature analysis was limited. Seasonal changes were analysed and very little variation were seen in the data, with a general decreasing trend with the profile depth.

Survey activities of the final field mission have also been summarised in the report. The survey included CTD data acquisition and sediment sampling. CTD casts from the three locations show similar trends of temperature along the profile depth.

4 References

About Education, Country Maps, http://geography.about.com/od/kiribatimaps/ accessed on 2nd December, 2015.

Battisti D.S. 1988. The dynamics and thermodynamics of a warming event in a coupled tropical atmosphere/ocean model. Journal of Atmospheric Science 45:2889–2919.

Battisti D.S, and Hirst A.C. 1989. Interannual variability in the tropical atmosphere–ocean model: Influence of the basic state, ocean geometry, and nonlinearity. Journal of Atmospheric Science 46:1687–1712.

Bosserelle C., Reddy S. and Lal D. 2015. Wave climate reports, Betio, Kiribati. Waves and Coasts of the Pacific (WACOP). 15 p.

Damlamian H., Bosserelle C., Kruger J., Raj A., Begg Z., Kumar S. and Baleilevuka A. 2015. Development of severe and extreme scenarios of wave and water level through statistical analysis and numerical modelling, Bonriki, Tarawa, Kiribati. SPC technical report.

Development of severe and extreme scenarios of wave and water level through statistical analysis and numerical modelling, Bonriki, Tarawa, Kiribati. SPC technical report, SPC00002.

Hirst A.C. 1986. Unstable and damped equatorial modes in simple coupled ocean atmosphere models. Journal of Atmospheric Science 43:606–630.

Holbrook J.N. and Bindoff L.N. 1998. Seasonal temperature variability in the upper southwest Pacific Ocean. Journal of Physical Oceanography, American Meteorological Society 29:366–381.

IPCC (Intergovernmental Panel on Climate Change). 2013. Annex III: Glossary (Planton S. ed). In: Climate change 2013: The physical science basis. Contribution of Working Group I to the Fifth Assessment Report of the Intergovernmental Panel on Climate Change. Stocker T.F., Qin D., Plattner G.-K., Tignor M., Allen S.K., Boschung J., Nauels A., Xia Y., Bex V. and Midgley P.M. (eds). Cambridge, United Kingdom: Cambridge University Press and New York, USA: Cambridge University Press.

Intergovernmental Committee on Surveying and Mapping. Permanent Committee on Tides and Mean Sea Level. 2011. Australian Tides Manual v4.1. Special Publication No. 9.

IPCC (Intergovernmental Panel on Climate Change). 2013. Annex III: Glossary ([Planton, S. (ed.)]. In: Climate Change 2013: The Physical Science Basis. Contribution of Working Group I to the Fifth Assessment Report of the Intergovernmental Panel on Climate Change. [Stocker, T.F., D. Qin D., Plattner G.-K., M. Tignor M., S.K. Allen S.K., J. Boschung J., A. Nauels A., Y. Xia Y., V. Bex V. and P.M. Midgley P.M. (eds.)]. Cambridge University Press, Cambridge, United Kingdom: Cambridge University Press and New York, NY, USA: Cambridge University Press.

Kessler W.S. Johnson G.C. and Moore D.W. 2003. Sverdrup and nonlinear dynamics of the Pacific equatorial currents. Journal of .Physical. Oceanography .33:, 994–1008.

Kruger J. and Sharma A. 2007. Kiribati Technical Report: High-resolution bathymetric survey in Kiribati. Fieldwork undertaken from 14 September to 19 October 2005. EUSOPAC Report 114.

Landsteiner M.C. McPhaden M.J. and Picaut J. 1990. On the sensitivity of Sverdrup transport estimates to the specification of wind stress forcing in the tropical Pacific. Journal of Geophysical Research-Oceans 95: 1681–1691.

Peter J. Leech P.J. Jean Lynch-Stieglitz J. and Rong Zhang R. 2013. Western Pacific thermocline structure and the Pacific marine Intertropical Convergence Zone during the last glacial maximum. Earth and Planetary Science Letters Elsevier, Volume 363: Pages 133–143.

Philander S. G. 1983. El Niño Southern Oscillation phenomena. Nature, 302, 295–301

Marks K.M. and Smith W.H.F. 2006. An evaluation of publicly available global bathymetry grids. Marine Geophysical Researches 27:19–34.

Munk W.H. 1950. On the wind-driven ocean circulation. Journal of Meteorology .7:79–93.

Naidu S. Aalbersberg W.G.L. Brodie J.E. Fuavao V.A. Maata M. Naqasima M. Whippy P. and Morrison R.J. 1991. Water quality studies on selected South Pacific lagoons. United Nations Environment Programme Regional Seas Reports and Studies No. 136, UNEP; and South Pacific Regional Environment Programme (SPREP) Reports and Studies No. 49.

OTEC News. http://www.otecnews.org/?_sm_au_=iTVN63fZQkFKStnP accessed on 15th December 2015.

Permanent Service for Mean Sea Level.
http://www.psmsl.org/data/obtaining/stations/1739.php accessed on 2nd December, 2015.

Philander S. G. 1983. El Niño Southern Oscillation phenomena. Nature 302:295–301.

Smith W. H. F. and D. T. Sandwell. 1997. Global seafloor topography from satellite altimetry and ship depth soundings, Science, v. 277, p. 1957-1962.

Sverdrup H.U. 1947. Wind-driven currents in a baroclinic ocean, with application to the equatorial currents of the eastern Pacific. Proceedings of the National .Academy of Science. USA 33: 318–326.

Talley L.D. Pickard G.L. Emery W.J. and Swift J.H. 2011. Descriptive physical oceanography, an introduction. 6th edition, Elsevier Press.

Pacific Community

Communauté du Pacifique